東京大学大学院新領域創成科学研究科
基盤科学研究系
先端エネルギー工学専攻

2004 年度修士論文

Experimental Study on Microwave Beaming Propulsion using a High Power Gyrotron

大電力ジャイロトロンを用いた マイクロ波ビーミング推進の実験的研究

学籍番号　３６２０３
氏名　　小田 靖久
指導教員　小紫 公也 助教授

（2005 年 2 月 14 日提出）

Acknowledgement

Author states an eventual and thankful acknowledgement to his advisers worthy of respect, Prof. Kimiya Komurasaki and Prof. Yoshihiro Arakawa.

Author is also grateful to Dr. Keishi Sakamoto, the chief of plasma heating laboratory at Japan Atomic Energy Research Institute(JAERI), and Prof. Tsuyoshi Imai, former chief of the laboratory and now at Tsukuba university, for research alliance of microwave beaming propulsion. Author is much obliged to Dr. Ryutaro Minami, Dr. Noriyuki Kobayashi, Dr. Koji Takahashi, and Mr. Atsushi Kasugai, the research stuffs of plasma heating laboratory at JAERI, for aids and advices for the experiments. Author also thanks Mr. Ikeda, Mr. Komori, and Mr. Ouchi, the laboratory technicians at JAERI, for operation of gyrotron system for our experiments.

Author wants to highlight all his friends for acknowledgement. However, allowed page for acknowledge is too few to list them all, thus only limited names are mentioned in following. Tatsuo Nakagawa, Makoto Matsui and Masato Ushio, members of Komurasaki laboratory, helped the author with experiments at JAERI. Akio Fukuda and Hiroshi Katsurayama, members of RP laser team at the laboratory, gave many advices to the author and helped with theoretical observation. Mr. Kashiwa from Ibaraki university, Mr. Owaki and Mr. Takado from Keio university, were author’s neighbors in Tokai village. Author shared joyful life in the rural research center with them.

Contents

List of Figures

List of Tables

Chapter 1

Introduction

1.1 Beamed Energy Propulsion

Beamed energy propulsion (BEP) is the system which gains propulsive energy by high power beamed electromagnetic wave transmitted from outside of the thruster. (Fig.1.1) Because BEP vehicles do not need to load an energy source, such as fuel tank and pump system, heavy electric source, or atomic reactor, the BEP propulsion thruster is very simple. And more, atmospheric air can be utilized as propellant through the flight in the atmosphere, the vehicle can achieve remarkably high payload ratio. As the propulsive energy is provided from the ground, the ground based beam station can be used for launch again and again. Therefore BEP technology is expected to realize extremely low-cost to-orbit-launch system.

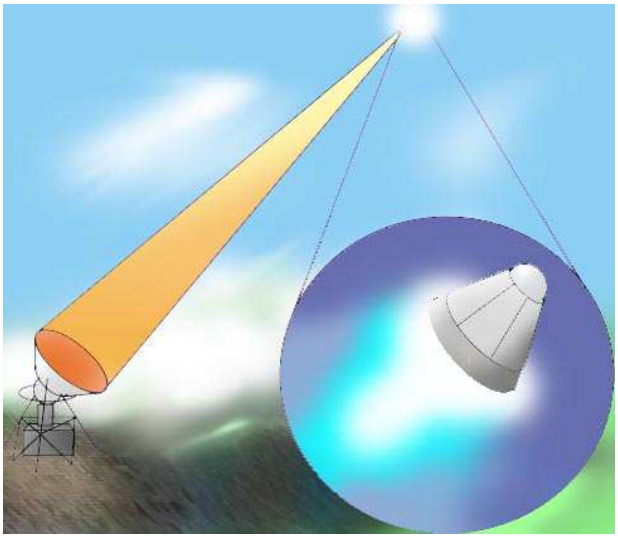

Figure 1.1: Illustration of beamed energy propulsion

1.1.1 Laser Propulsion

In open technical literatures, Kantrowitz first proposed in 1972 the concept of launching object using a laser power supplied from a ground-based device.[1] Since that time, laser beamed energy propulsion has intensively been nominated as a promising method of transporting vehicles with a vastly-low cost. In 1970s, Pirri measured the characteristics of laser-driven impulse generated with a parabolic reflector.

Currently a majority of researches of BEP is devoted on laser propulsion. The utilizations both of continuous wave(CW) laser and of repetitive pulse (RP) laser have been investigated.

As high power laser oscillator was developed in recent years, experimental studies were held in U.S.A., Europe, Russia, China and Japan.

The most famous experiment in laser propulsion was conducted by L.Myrabo et al. in U.S.A.. They launched vertically a small duralmin thruster model with parabolic nozzle called "lightcraft". In 2000, they had achieved 71m height flight using 10kW-average repetitive pulsed laser.[2][3]

1.1.2 Microwave Beaming Propulsion

The concept of our microwave-beaming propulsion is very similar to repetitive-pulse laser beaming propulsion: (Figure 1.2) A vehicle focuses the transmitted microwave beam by a parabola reflector and causes breakdown of atmospheric air in the vicinity of the focal point. The induced plasma absorbs the following part of beamed energy and expands outwards while generating a shock wave. The nozzle surface of the thruster reflects the shock wave, and the vehicle gains impulsive thrust.

Microwave-beaming has some advantages in comparison with laser-beaming: 1) The development cost of microwave generators is generally two-orders lower than that of laser oscillators. 2) A single beam at the power level of GW will be obtained by clustering microwave generators with the use of phased array technology.

The concept of microwave rocket was proposed as early as 40 years ago. In the early concept of microwave BEP, a continuous microwave beam was thought used for propellant heating.[4][5]

However, the experimental study of microwave BEP was not conducted for long time. Because the wave length of microwave is very long compared to laser, a microwave BEP thruster requires very large reflector to focus the microwave beam propagated for long range.

The scale of the thruster is determined from wavelength of microwave. So high-frequency microwave, especially millimeter-wave, is necessary to apply for microwave BEP. However, high power millimeter-wave generator was not invented for a long time. Recently, as high-power gyrotrons are developed, experimental study on microwave BEP have started.

In 2002, Nakagawa et al. achieved 2-m flight experiment using a 1-MW gyrotron.[6]

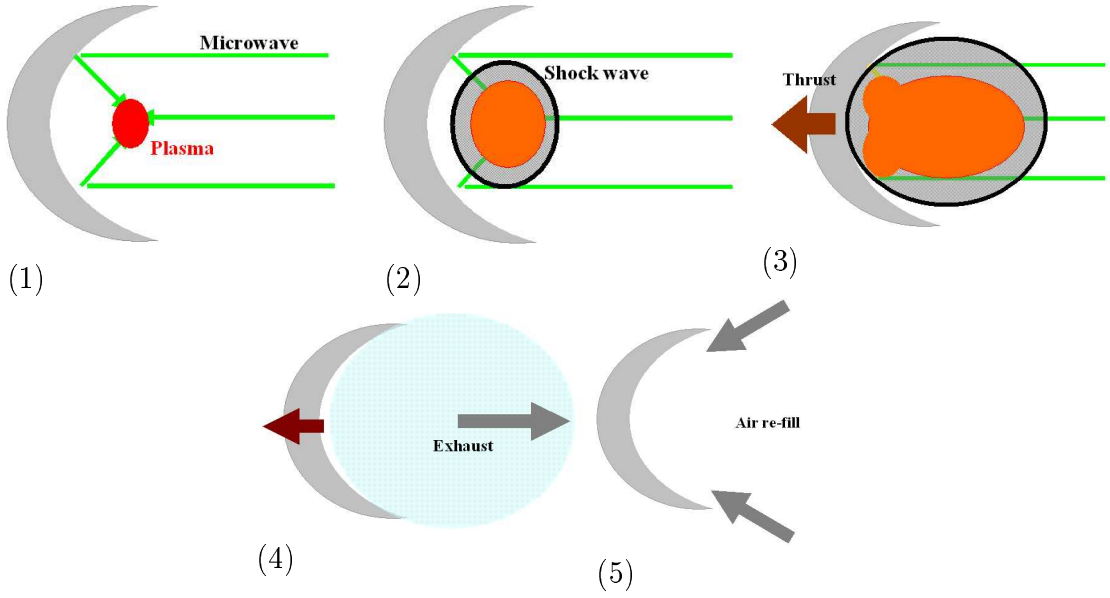

Figure 1.2: Schematics of the concept of Microwave Beaming Propulsion: 1) A parabola reflector focuses the microwave beam and causes breakdown of atmospheric air. 2) The induced plasma absorbs the microwave energy and expands outwards while generating a shock wave. 3) The nozzle reflects the shock wave. 4) Exhaust from the nozzle. 5) Air refill process. The vehicle gains thrust through 3)-4) process.

1.1.3 Feasibility Study

Microwave Beam Transmittion

Microwave propagates long distance to provide energy to launch vehicle, for application for BEP launch system. As an electromagnetic beam propagates long distance, beam spot diverges a lot. Diverged spot radius of long propagated electromagnetic beam is obtained equation 1.1 for 0th Gausian mode.

$$w(z) = w_0\sqrt{1+\left(\frac{\lambda z}{\pi w_0^2}\right)} \tag{1.1}$$

Table 1.1 lists the necessary beam radius at groud based station to provide energy to the vehicle. We assumed a vehicle with a reflector of 5m-diameter flying at 100km altitude.

Transparency of Atmosphere

Application of microwave to beamed energy propulsion is limited to frequencies at which the atmosphere is transparent. A research by K.Parkin mentioned on microwave beam propagation through atmosphere.[7]

The advent of submillimeter astronomy has highlighted the existence of locations with particularly low atmospheric water content, opening up new microwave transmission win-

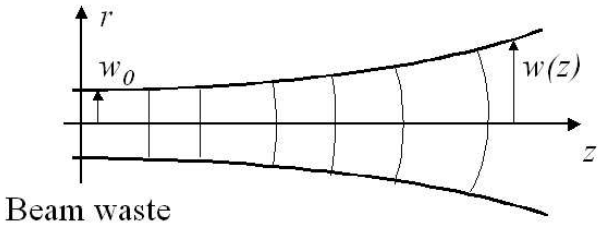

Figure 1.3: Schematic figure of beam spot

Beam	wavelength	beam radius
Millimeter-wave (170GHz)	1.7mm	22m
CO_2 Laser	10μm	2.5m
ISM Microwave (2.45GHz)	12cm	1,500m

Table 1.1: Comparison of beam spot radius for the vehicle with 5m-reflector at 100km altitude

dows between 35-300GHz and sometimes beyond. Since the atmospheric scale height of water vapor is only 1-2km, sites such as the Caltech Submillimeter Observatory (CSO) on Mauna Kea are at high altitude, where atmospheric water vapor levels permit transmission above 250GHz, shown in Fig.1.4

Launch Cost

Katsurayama et al. analytically examined feasibility of SSTO system powered by RP laser and microwave. They proposed a vertical launch to minimize the development cost of the laser base. (Fig.1.5) The vehicle is boosted by beaming propulsion to reach the orbit beyond the GEO. At the apogee point, the vehicle is kicked to a GTO by on-board motor and deccelerated at the perigee point as well.

This research considered on the construction of a 100-ton space solar power satellite in GEO. If 1GW-output microwave facility becomes available, a vehicle can launch 100kg payload. Along to their consideration, 1,000 launches are necessary, and cost becomes almost one-tenth of chemical rocket's cost.[9][8]

1.2 High-power Microwave Generator

Microwave generator is categorized into two types, vacuum tube type and solid-state type. For high power application, vacuum tubes have achieved much higher power level than solid-state.

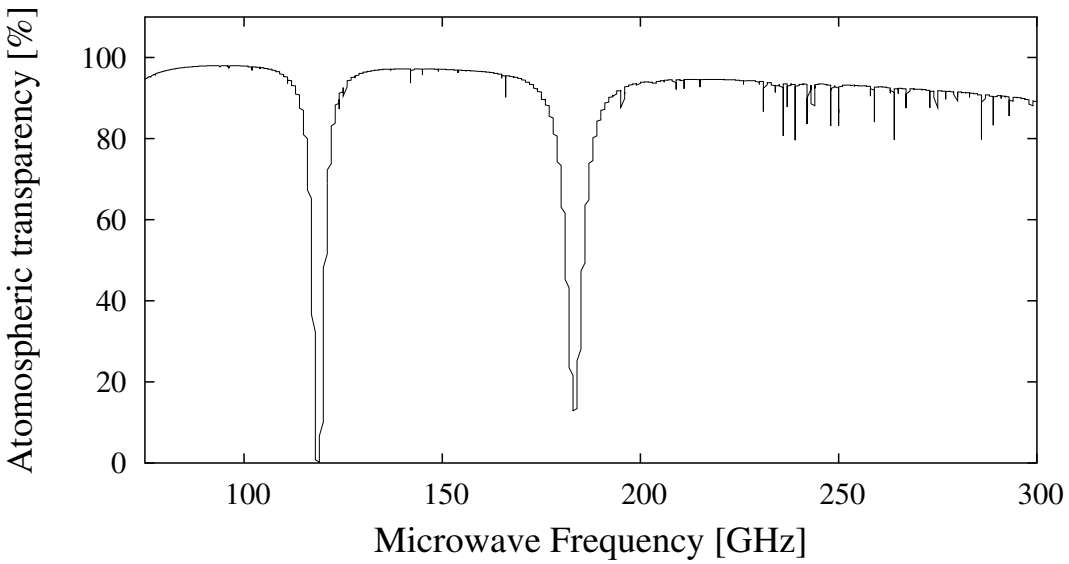

Figure 1.4: CSO atmospheric transmission from Mauna Kea calculated typical water content, using (http://www.submm.caltech.edu/cso/weather/atplot.shtml). Precipitable Water Vapor: 1mm.

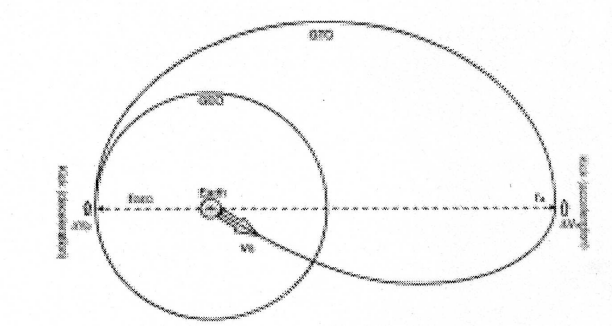

Figure 1.5: Trajectory to GEO[8]

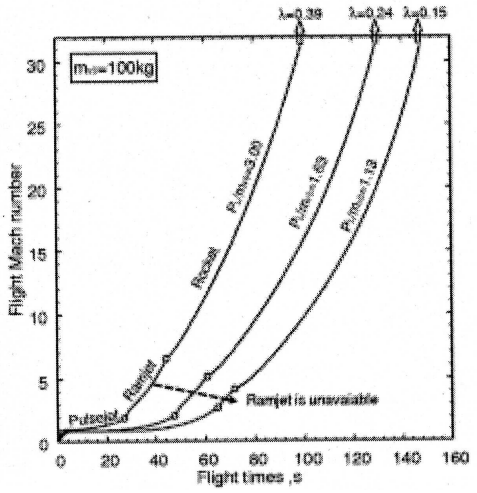

Figure 1.6: Flight Mach number vs. flight time[8]

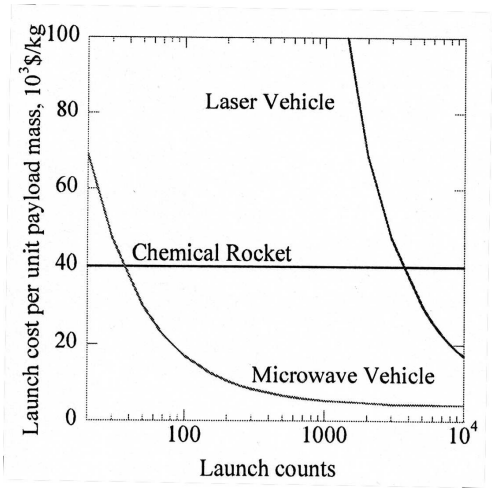

Figure 1.7: Launch Cost[8]

1.2.1 Convenctional Microwave Power Tube

Magnetron

Magnetrons are the most familiar microwave device. In the magnetron, a layer of electrons rotates azimuthally in the coaxial space between inner cathode and an outer anode due to the combined effect of radial dc electric field and axial dc magnetic field. The anode contains a number of coupled resonant cavities arranged periodically around the azimuth. The interaction between an azimuthally traveling wave associated with the coupled cavities and the synchronously rotating electron layer produces electron velocity modulation, bunching and microwave power generation. Magnetrons are easily fabricated and have been of great military and commercial significance.

Klystron

Klystrons are basic microwave devices based on coherent transition radiation of electrons. The klystron in its simplest embodiment consists of a gun injects a linearly propagating electron beam at a energy corresponding to the full anode voltage through a circuit consisting of two resonant cavities separated by a drift tube. The first resonant cavity is excited by an input microwave signal. The electron beam then passes through a short interaction space between grids in the input cavity. The transit time of each electron across the interaction space is small compared with a period of the microwave signal, and the velocity modulation of a particular electron depends on the magnitude and orientation of the microwave field it encounters in the interaction space. In the field-free drift tube following the input cavity, faster electrons overtake slower electrons, and the electrons form bunches in space along the flow axis. This bunched electron beam then excites microwave as it passes through a short interaction space in an output cavity (transition radiation) from

which a microwave signal may be extracted that is much more powerful than the input signal.

TWT (Traveling Wave Tube)

The TWT employs an electron gun similar to that in a klystron to inject an axially streaming electron beam into a periodic slow-wave structure along which can travel electromagnetic waves that have a phase velocity early equal to the electron velocity. The distributed interaction between the electrons and the traveling wave can lead to electron velocity modulation, spatial bunching, and wave amplification over a wide frequency band. Thus, TWTs have been extensively developed for wideband applications and especially for radar jammers(electronic warfare).

These devices, which depend on electron velocity modulation and spatial bunching, can be seen to extend frequency range for high-power microwave generation by about one and a half orders of magnitude beyond gridded tube capabilities. However, they also eventually decrease in power rating as frequency increases, especially for frequencies above 10 GHz. The principal reason is that the dimensions of the interaction circuit must be small compared with the wavelength, leading to excessive heating when average power becomes too large and electrical breakdown at high peak power.[10]

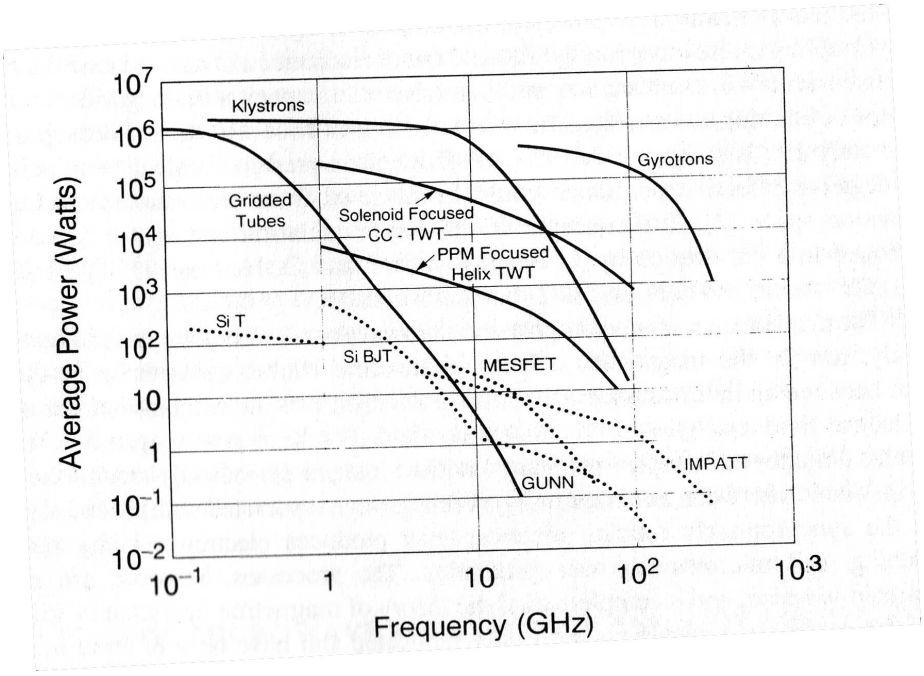

Figure 1.8: View of Microwave Power Source Technology[10]

1.2.2 High Power Gyrotron

Recent progress in the increase in power and frequency of microwave sources has been caused by the development a new branch of physics which can be called high-frequency relativistic electronics. By this term we mean the appearance of microwave sources either based in relativistic effects or using beams of relativistc electrons. Among microwave tubes based on electron bremsstrahlung radiation in a constant magnetic field, the most common are CRMs(cyclotron resonance maser) or gyrodevices.

The process of phase bunching and energy transfer in CRMs can be better appreciated by referring to Figure 1.9. In Figure 1.9, we see electrons in a magnetic field B_0, executing circular orbits with radii equal to the Larmor radius r_L. The frequency of the rotation is the electron cyclotron frequency Ω. As shown in Figure 1.9, the electrons are homogeneously distributed over their inital phases. In the presence of a traveling electric field E rotating synchronously with electrons as would be found in a microwave cavity or waveguide, the electrons gain or lose energy depending on the sign of $E \cdot v$, where v is the electron velocity. Due to the energy dependence of the frequency of electron oscillation Ω, it will be increase or decrease depending on whether energy is lost or gained, resulting in phase bunching.

The electron cyclotron frequency Ω is described as,

$$\Omega = \frac{eB_0}{m_0\gamma} \tag{1.2}$$

here, B_0 static magnetic field, $m_0\gamma$ relativistic mass of electron. $\gamma = (1 - v^2/c^2)^{-1/2}$ is the relativistic Lorentz factor for electrons, v is electron velocity and m_0 is the rest mass of an electron.

If the microwave frequency is slightly higher than the cyclotron frequency, the resulting phase bunching in the cyclotron orbit occurs in the decelerating phase of the wave. Then $v \cdot E$ is positive quantity for most of the electrons, they lose energy, and there is a net transfer of energy from the electron orbital motion to the microwave field.

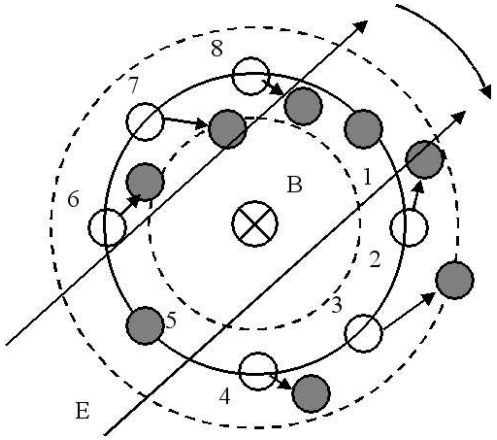

Figure 1.9: Schematic figure of cyclotron resonance maser

The cyclotron resonance maser instability depicted in figure 1.9 was first described

in 1958-59 in the independent work of four scientists, namely, RO.Twiss in Australia, J.Schneider and R.H.Pantell in the United States, and A.V.Gaponov-Grekhov in the USSR. However, the first development of the gyrotron oscillator, a practical cyclotron resonance maser configuration, was invented and first developed in the USSR. Figure 1.10 shows the configuration of typical gyrotron. This involved a magnetron injection gun producing an annulus of electrons following helical path along the lines of an axial magnetic field, and a single, open-ended, resonant cavity into which the spiraling electrons were injected.

In the cavity, the electrons interacted with the microwave field and experienced both phase bunching and transfer of energy to the field. An important advantage of this configuration is the complete separation of the interaction space from the electrodes forming the electron the electron flow. Thus, there is no restriction on operating voltage due to the requirements of avoiding electrostatic breakdown in the interaction space.

In contrast to other microwave devices, the interaction circuit is a high-order-mode cavity allowing higher power at higher-frequency. Their present average power capabilities are plotted versus frequency in Figure 1.8, where they can be seen to extend the frequency range of high-power microwave generators by about an order of magnitude compared with the conventional generators based on spatial bunching principles.[10]

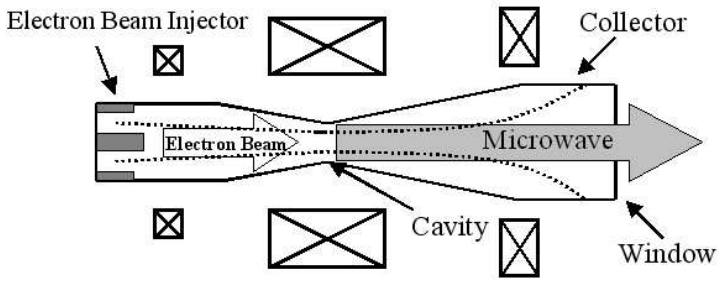

Figure 1.10: Configuration of gyrotron

At present gyrotrons are mainly used as high power millimeter-wave sources for electron cyclotron resonance heating(ECRH), electron cyclotron current drive(ECCD), stability control and diagnostics of magnetically confined plasmas for generation of energy by controlled thermonuclear fusion.

The maximum pulse length of commercially available 1.0MW gyrotrons employing open-ended cylindrical resonators and synthetic diamond output windows is 5sec at 110GHz, 12sec at 140GHz and 9sec at 170GHz, with efficiencies slightly above 30%. The energy world record of 160MJ(0.89MW at 180s pulse length and 140GHz) at power levels higher than 0.8MW has been achieved by European FZK-CRPP-CEA-TED collaboration. Total effciency around 50 % have been obtained using a single-stage depressed collector(SDC).

A maximum output power of 2.2MW at 165GHz(1mse pulse length) was obtained at FZK with an efficiency of 28%.[11]

The gyrotron of high electric efficiency was developed at Tsukuba university and Japan Atomic Energy Research Institute, their 28GHz-0.5MW gyrotron archieved 50% efficiency without depressed collector.[12]

For high frequency devices, IAP developed 650GHz-40kW gryrotron and Fukui university achieved highest frequency 890GHz using 0.1kW gyrotron.

Chapter 2

Atmospheric Microwave Plasma

2.1 Microwave Plasma Propagation

Plasma formed on high power microwave develops along the microwave beam channel, absorbing microwave power. Figure 2.1 shows typical photograph taken 170GHz 700kW, 0.4msec condition.

Researches on the atmospheric discharge caused by high power millimeter-wave were conducted in Russia. Propagation velocity of discharge front depends on microwave power flux density.[13] When propagation velocity is small, the heat transfer model, which is similar to slow combustion model, explains dependency well.[14] However, in high power density condition, the propagation velocity comes up to super sonic. Brodskii et al proposed a plasma-front propagation model based on photo-ionization in the plasma front region. In his model, air is assumed ionized through a discharge plane, and microwave is partly absorbed and partly reflected at the plane without leakage. The reflection is governed by plasma parameters at the plane. Mnatsakanian et.al. and Sizykh solved the problem of discharge propagation numerically in a one-dimensional approximation and calculated the velocity for the condition of Brodskii et al. [15][16][17]

2.2 Interaction Between Plasma and Shock Wave

The propagating plasma in super sonic velocity is considered to form a shockwave. This section shows the model of propagating plasma with shock wave. In this model, microwave power is assumed to be absorbed in a post-shock layer.

Figure 2.3 shows schematic of plasma propagation model. Here, v_1 is flow velocity, ρ_1 is density, p_1 is pressure, T_1 is temperature in pre-shock region. v_2, ρ_2, p_2, and T_2 are gas properties in post-shock region. The gas properties in pre-shock and post-shock layers are related by following conservation laws.

$$\rho_1 v_1 = \rho_2 v_2 \tag{2.1}$$

$$p_1 + \rho_1 v_1^2 = p_2 + \rho_2 v_2^2 \tag{2.2}$$

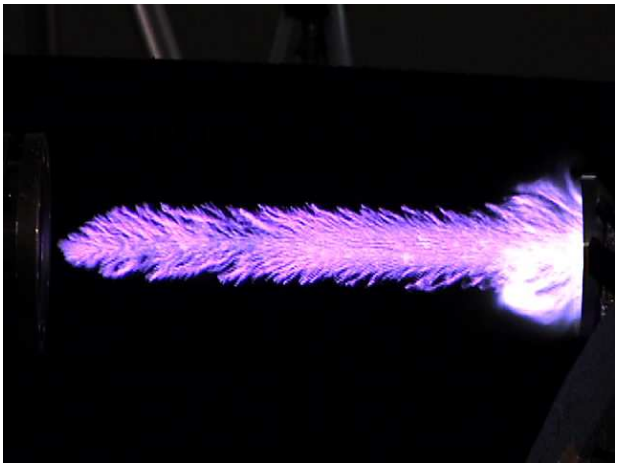

Figure 2.1: Photograph of Microwave Plasma, 700kW, τ=0.4msec

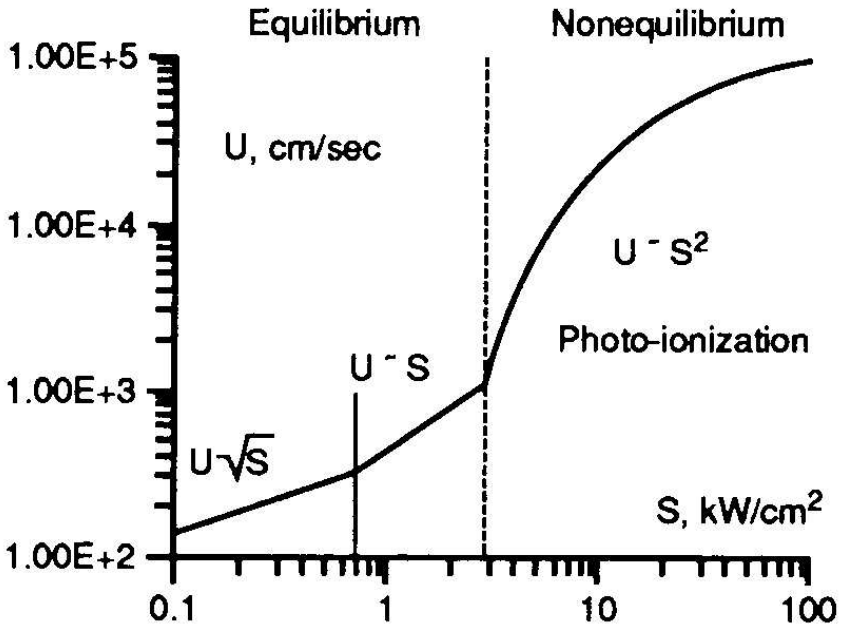

Figure 2.2: Dependence of discharge propagation speed versus microwave power flux

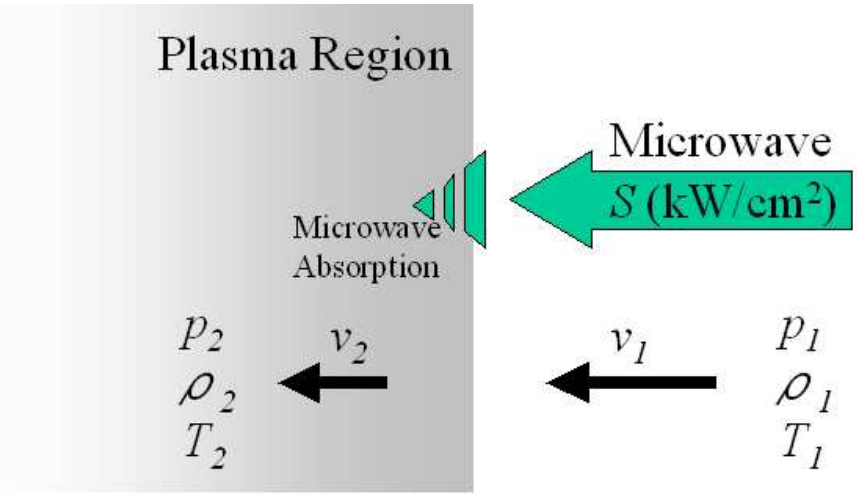

Figure 2.3: Plasma propagation model

$$h_1 + \frac{1}{2}v_1^2 + q \;\; = \;\; h_2 + \frac{1}{2}v_2^2 \tag{2.3}$$

Here, h is enthalpy that is function of temperature T, and q is absorbed energy. q is related with microwave power flux density S as

$$q\rho_1 v_1 = \eta S \tag{2.4}$$

where η is fractional absorption which is connected to the reflection by plasma. Heat conduction and direct photo-ionization by ultra-violet radiation transfers absorbed heat to pre-shock air. However, the ratio of heat conduction to radiation is not clarified yet. Here, instead of an equation of energy transfer, Chapman-Jouget condition was applied. Using specific volume $V = 1/\rho$ and Eq. 2.2, we obtain

$$v_1 = jV_1 \qquad v_2 = jV_2 \tag{2.5}$$

and substitute this into Eq.2.1,

$$j^2 = \frac{p_2 - p_1}{V_1 - V_2} \tag{2.6}$$

Next, substituting Eq.2.5 into Eq.2.1, we obtain

$$h_1 + \frac{1}{2}j^2V_1^2 + q = h_2 + \frac{1}{2}j^2V_2^2 \tag{2.7}$$

Assuming caloric ideal gas, enthalpy h is expressed as following,

$$h = h_0 + C_{\mathrm{p}}T = h_0 + \frac{\gamma}{\gamma - 1}pV \tag{2.8}$$

substitute this into Eq.2.7,

$$\frac{\gamma_2 + 1}{\gamma_2 - 1}p_2V_2 - \frac{\gamma_1 + 1}{\gamma_1 - 1}p_1V_1 - V_1p_2 + V_2p_1 = 2q \tag{2.9}$$

We obtain following expressions for properties in plasma region from Chapman-Jouget condition.

$$j^2 = \gamma_2\frac{p_2}{V_2} = v_1/V_1 \tag{2.10}$$

$$p_2 = \frac{p_1 + j^2V_1}{\gamma_2 + 1} \tag{2.11}$$

$$V_2 = \frac{\gamma_2(p_1 + j^2V_1)}{j^2(\gamma_2 + 1)} \tag{2.12}$$

Substituting these expressions into Eq. and replacing j by v_1/V_1, we obtain biquadratic equation for the velocity v_1:

$$v_1^4 - 2v_1^2((\gamma_2^2 - 1)q + (\gamma_2^2 - \gamma_1)c_vT_1) + \gamma_2^2(\gamma_1 - 1)^2c_{\mathrm{v}1}^2T_1^2 = 0 \tag{2.13}$$

where the temperature has been introduced by $T = pV/c_{\mathrm{v}}(\gamma - 1)$. Hence,

$$\begin{aligned} v_1 &= \sqrt{(\gamma_2 - 1)((\gamma_2 + 1)q + (\gamma_1 + \gamma_1)c_{\mathrm{v}1}T_1)/2} \\ &+ \sqrt{(\gamma_2 + 1)((\gamma_2 - 1)q + (\gamma_2 - \gamma_2)c_{\mathrm{v}1}T_1)/2} \end{aligned} \tag{2.14}$$

After all, the equation which relates velocity to pressure ratio is conducted as follows: [18]

$$\frac{p_2}{p_1} = \frac{v_1^2 + (\gamma_1 + 1)c_{\mathrm{v}1}T_1}{(\gamma_2 + 1)(\gamma_1 - 1)c_{\mathrm{v}1}T_1} \tag{2.15}$$

If pressure at plasma region p_2 is assumed invariant to ambient pressure, dependency of plasma propagation velocity v_1 on ambient pressure p_1 is calculated using Eq.2.15. In this study, p_2 estimated by velocity of plasma propagation at 1atm was used.

Chapter 3

Experimental apparatus

3.1 High Power Microwave Generator

A gyrotron microwave oscillator developed by the Japan Atomic Energy Research Institute was used in this study.(Fig.3.1) This microwave sources have been developed for International Thermonuclear Experimental Reactor (ITER). Its specifications are listed in Table 3.1. Output power P is almost constant during the pulse duration τ.(Fig.3.3) In the gyrotron, the microwave is oscillated through the interaction between accelerated electron beams and electromagnetic waves by a cyclotron resonance maser in a cavity with magnetic fields.[19][20]

Frequency	170GHz
Output Power P	$\leq$ 1MW
Pulse Duration τ	0.1ms - 10s
Beam profile	Gaussian
Beam waist	38mm
Electrical efficiency	50%

Table 3.1: JAERI gyrotron specifications

Microwave was guided to the launch site using a corrugated waveguide. A microwave beam was transmitted from the waveguide outlet through a diamond window.(Fig.3.4) The beam profile was 0th order Gaussian and its beam waist was 38mm. Figure 3.6 and 3.7 shows the measured beam profile.

In the middle way of waveguide, a microwave detector was settled with a directional coupler and microwave power was measured. The reference power of microwave was measured using a directional coupler, where the power was calibrated with a calorimetric measurement using dummy load.

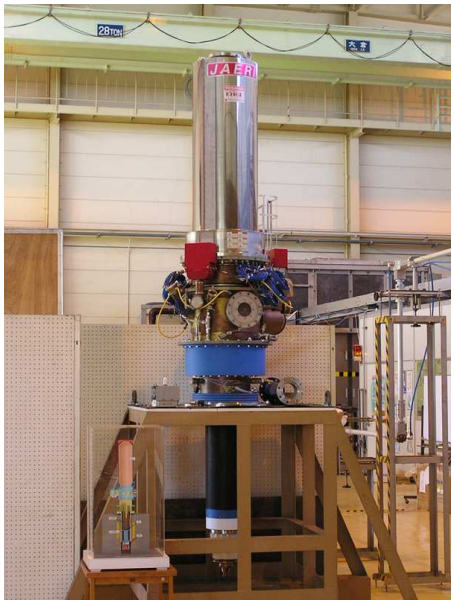

Figure 3.1: 170GHz 1MW-class gyrotron, JAERI

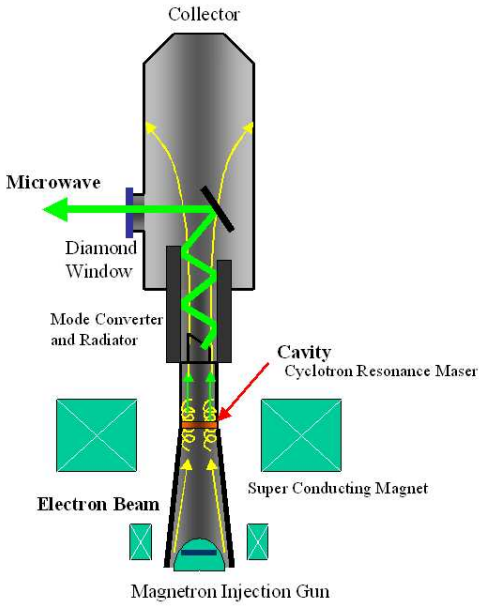

Figure 3.2: Configuration of JAERI gyrotron

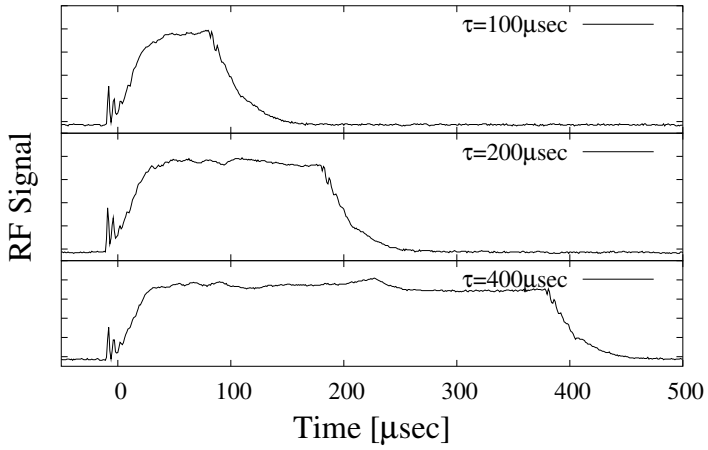

Figure 3.3: Typical signals of microwave pulse

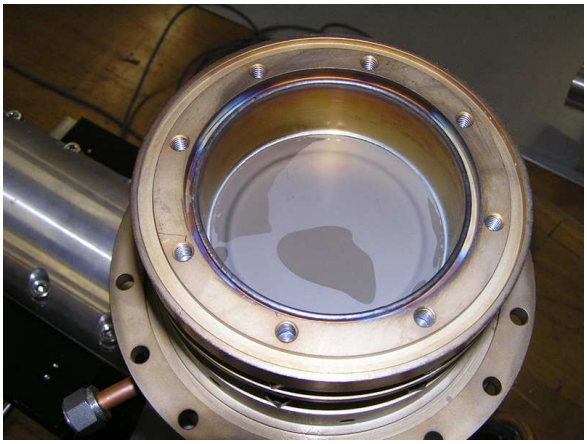

Figure 3.4: Diamond window set to the end of waveguide

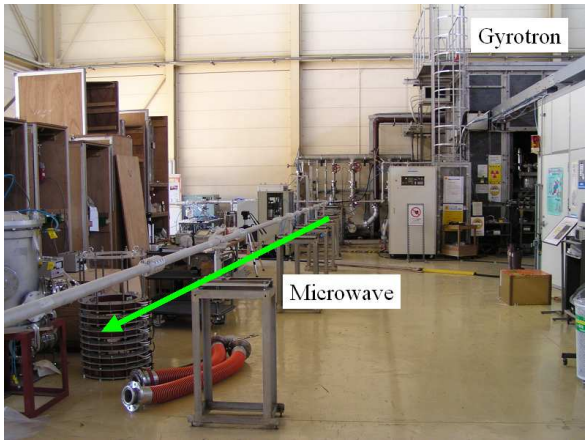

Figure 3.5: Microwave transmiitted to the lauch site using a corrugated waveguide

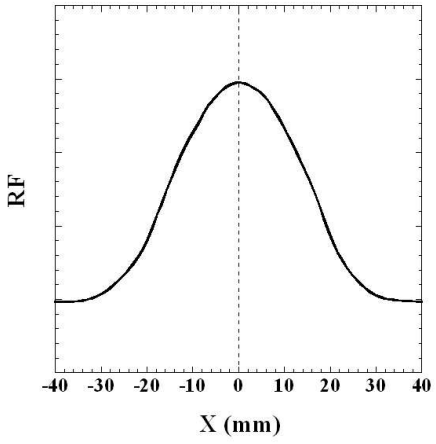

Figure 3.6: Measured radial beam profile, 120GHz, measured at 600mm from the end of corrugated waveguide

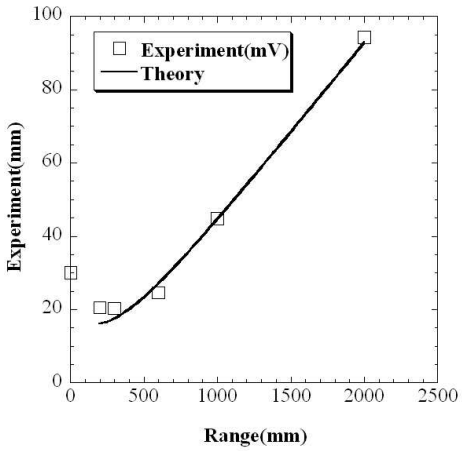

Figure 3.7: Measured beam divergence, 120GHz

Multi Pulse Operation

To provide microwave pulses repetitively, acceleration voltage of an electron beam was modulated and oscillation mode in the cavity was controlled.

A typical signal of microwave pulse is shown in Fig.3.8. The width of each microwave pulse was about 1msec, though peak power was varied as listed in Table 3.2.

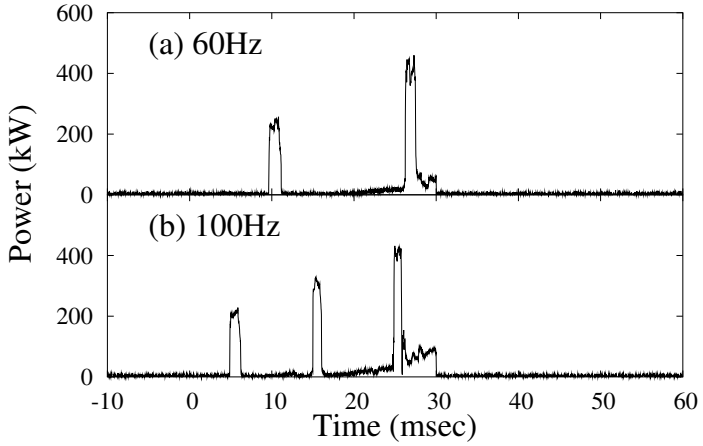

Figure 3.8: A typical microwave signal, (a) 60Hz, 2pulse / (b) 100Hz, 3pulse

Repetition	Microwave Power (kW)		
rate (Hz)	1st pulse	2nd pulse	3rd pulse
60	257	452	
100	266	350	470

Table 3.2: Microwave power at each pulse

3.2 Thruster Model

In this study, three types of thruster models were used.

Parabola Thruster Model

A thruster model has a parabolic reflector whose diameter and focal length are 90mm and 15mm, respectively. It is made of duralumin and weighs 100g. The thruster model is plated with copper.

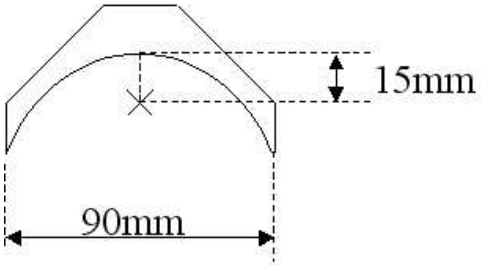

Figure 3.9: Configuration of parabola thruster model

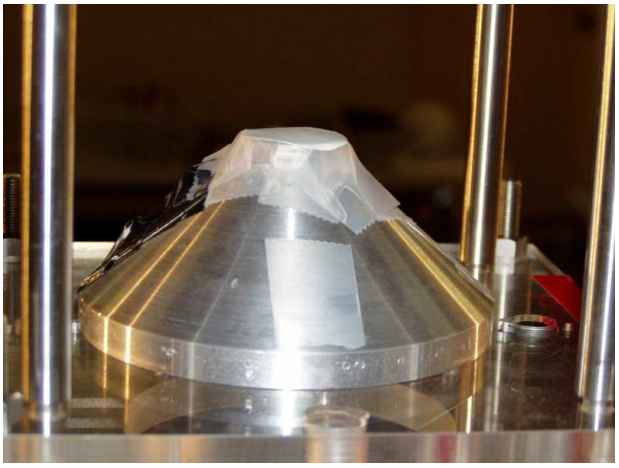

Figure 3.10: Parabola thruster model

Cone-Cylinder Thruster Models

A conical nozzle with a cylinder body of variable length was made, as shown in Figures 3.11 and 3.12. Body length L was varied from 0mm to 120mm and corresponding model weight was varied listed in Table 3.3. The inner surface of the cone was covered with aluminum foil. Although a cone does not focus a microwave beam tightly, we ignited plasma successfully with no misfiring.

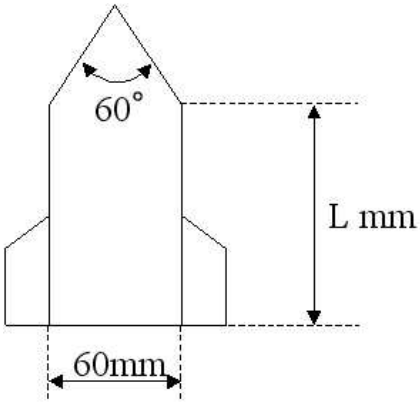

Figure 3.11: Configuration of cone-cylinder thruster model

Figure 3.12: Cone Cylinder Thruster models

Cone Thruster Models

Conical thruster models(3.13 and 3.14) were also used with various half-cone angle α and nozzle length R_n along a generation line of a cone. Table 3.4 lists specifications of cone type thrusters. The inner surface of the cone was covered with aluminum foil.

Legth of Body (mm)	Weight (g)
0	4.5
60	13
90	18.4
120	19.4

Table 3.3: Specifications of cone-cylinder thruster models

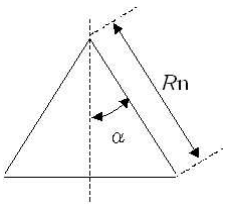

Figure 3.13: Configuraiton of cone thruster model

Figure 3.14: Cone thruster models

Half Cone Angle α degree	Diameter D (mm)	Nozzle Length R_n (mm)	Weight m (g)
30	90	90.0	41.7
30	60	60.0	24.3
30	40	40.0	7.5
45	90	63.6	27.9
45	60	42.4	15.3
45	40	28.3	4.9
60	90	52.0	19.7
60	60	34.6	7.9
60	40	23.1	6.3

Table 3.4: Specifications of cone thruster models

3.3 Meathod of Thrust Measurement

3.3.1 Thrust Stand

Thruster models were launched vertically and flight trajectories were recorded using a laser displacement gauge. Figures 3.15 and 3.16 shows the setting of the launche site.

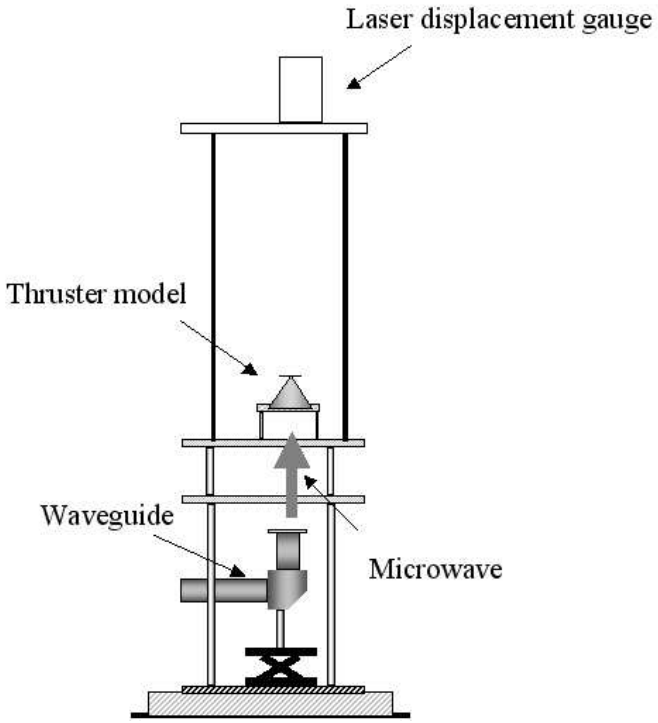

Figure 3.15: Measurement apparatus settings

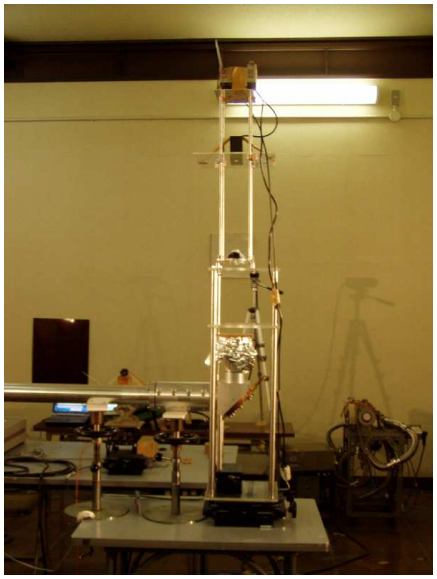

Figure 3.16: Photograph of launch site in sealed room

3.3.2 Reduced Pressure Chamber

Experiments were carried out under the ambient pressure of 0.1-1atm using a cubic chamber with a 30cm side. (Figs.3.17 and 3.18) The chamber had optical windows on the top and side for observation. The chamber pressure was measured by a crystal pressure gauge(ANELVA Crystal Gauge M-320XG). The microwave was launched into chamber from the bottom of it.

A couple of windows were settled on the way of waveguide for sealing.

3.3.3 Flight Trajectory

In this study, two laser displacement gauges were used. The long ranged gauge (KEYENCE LK-500) was applied at the atmospheric thrust stand, and a short ranged gauge (KEYENCE

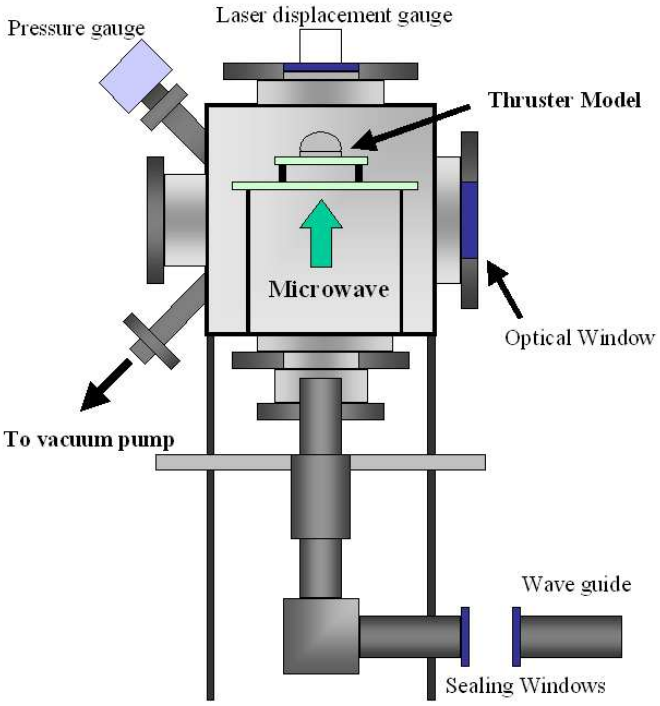

Figure 3.17: Schematic of a chamber setup

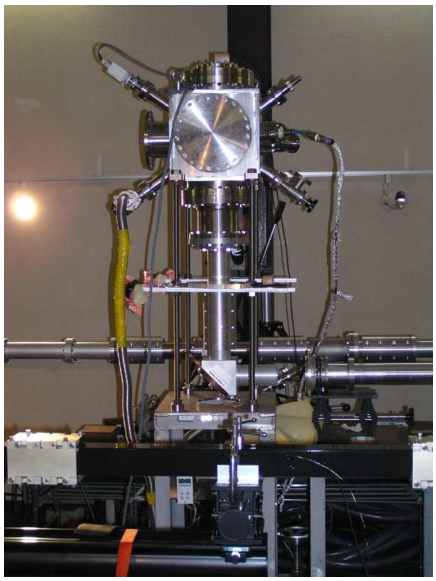

Figure 3.18: Photograph of reduced pressure chamber

LB-01) with small sensor head was applied at reduced pressure chamber experiment. The sensor signal was recorded using a digital oscilloscope.

Propulsive impulse was calculated from flight altitude h at single pulse operation. Indeed, at multi pulse operation, the initial velocity v was calculated from the trajectory and impulsive thrust estimated for pulse by pulse. Impulse was calcuated using,

$$I = m\sqrt{2gh} = mv \tag{3.1}$$

where m and g represent vehicle mass and gravitational acceleration, respectively. Typical multi-pulsed flight trajectory is shown in Fig.3.19.

3.4 Plasma and Shock Wave Observation

Photographs of plasma development in microwave channel were taken using a high-speed framing camera (PHOTRON LTD. FASTCAM ultima 40K), shown in Fig.3.20. The maximum framing speed was 40,500 frames per second. The plasma propagation velocity was deduced from the images.

The propagation velocity of shock waves directed to the reflector was measured using high-speed pressure gauges (piezo sensors:Fuji Ceramics 3Z 5D-SY1 C 63) fixed on a parabola surface as shown in Figures 3.21 and 3.22. Typical gauge signal is shown in Figure **??**.

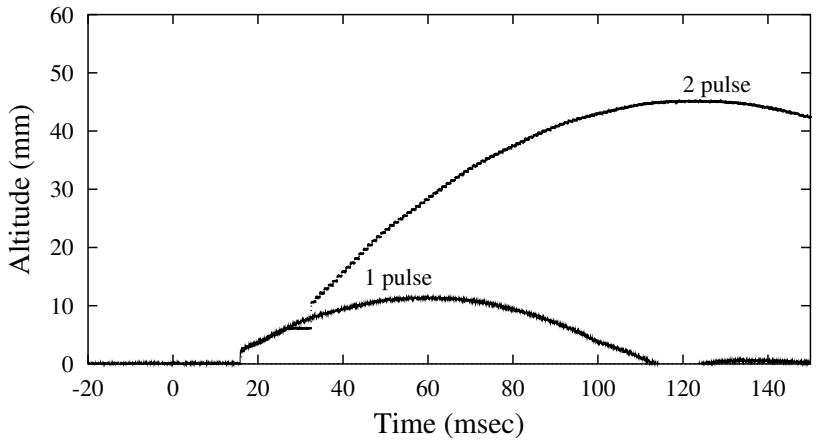

Figure 3.19: Measured flight trajectory

Figure 3.20: Fast Framing Camera: FASTCAM ultima 40K, PHOTORON LTD.

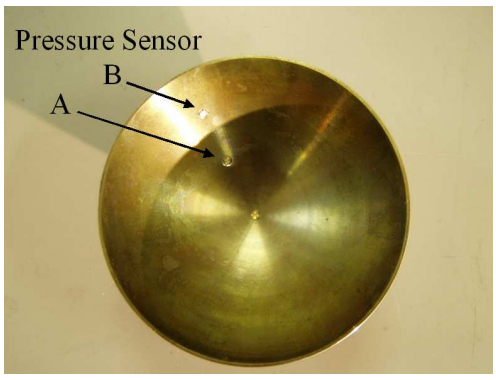

Figure 3.21: Photograph of pressure sensors

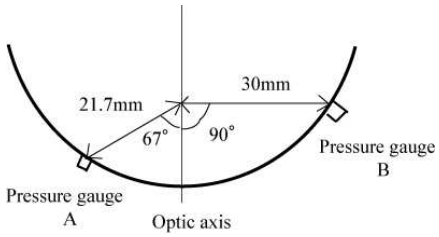

Figure 3.22: Location of piezo sensors

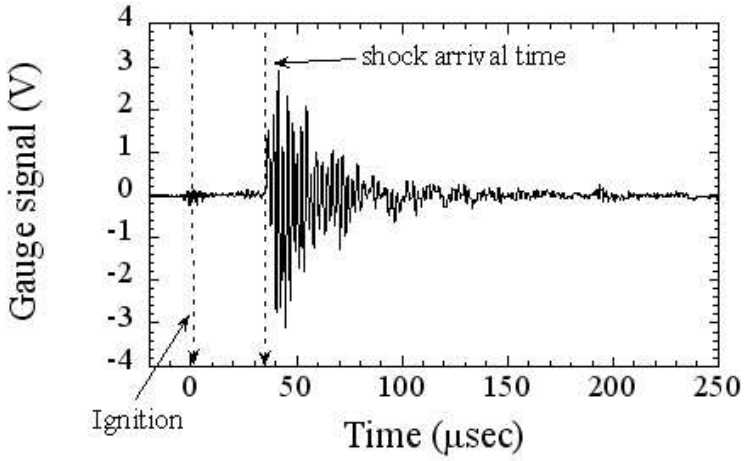

Figure 3.23: Typical pressure gauge signal. P=930kW, 170GHz, τ=0.2ms

Figure 3.24 shows measurement apparatus setup.

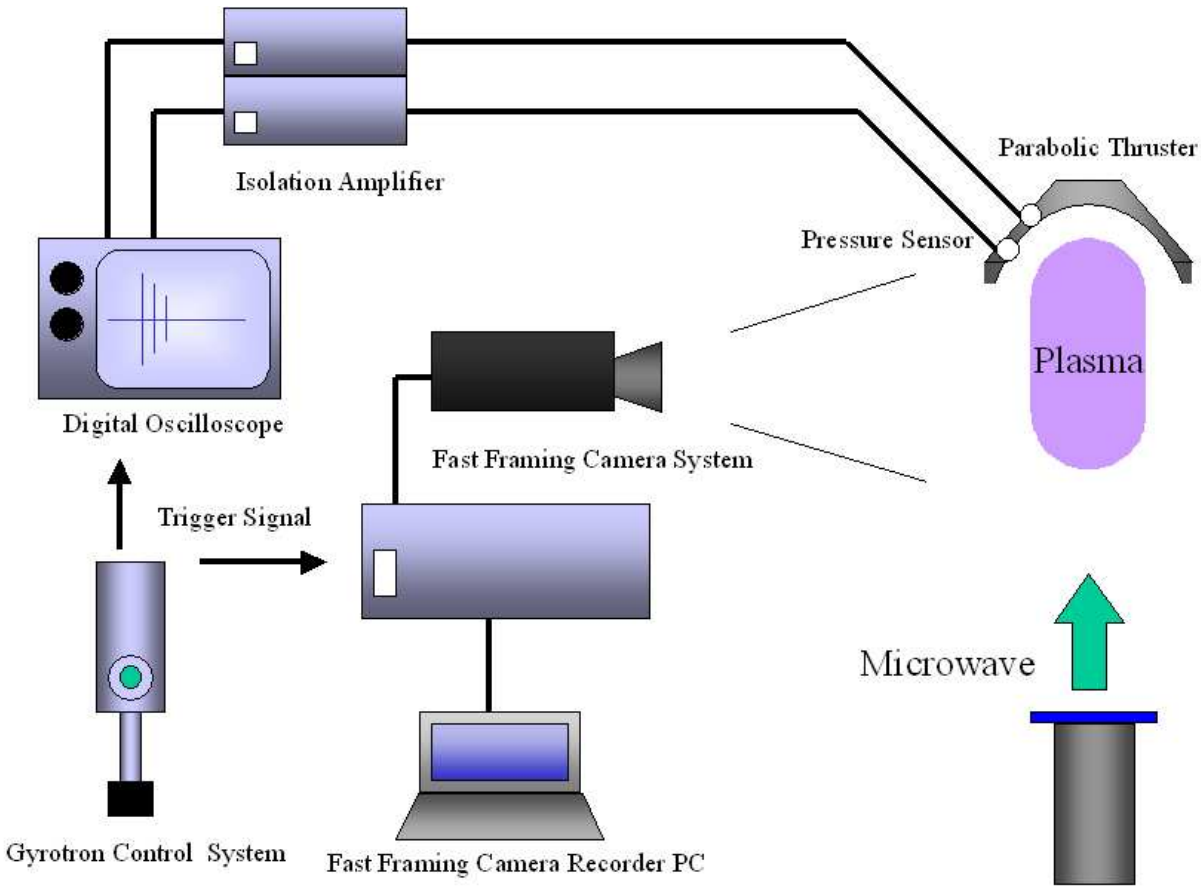

Figure 3.24: Measurement Apparatus Setup

Chapter 4

Experimental Result

4.1 Plasma and Shock Wave Propagation

4.1.1 Discharge front propagation in a parallel microwave channel

Figure 4.1 shows side-view pictures of plasma development taken using a high-speed framing camera. A parabola model was used for plasma ignition. As seen in the figure, the plasma front propagates toward the upstream of microwave beam at a constant velocity.

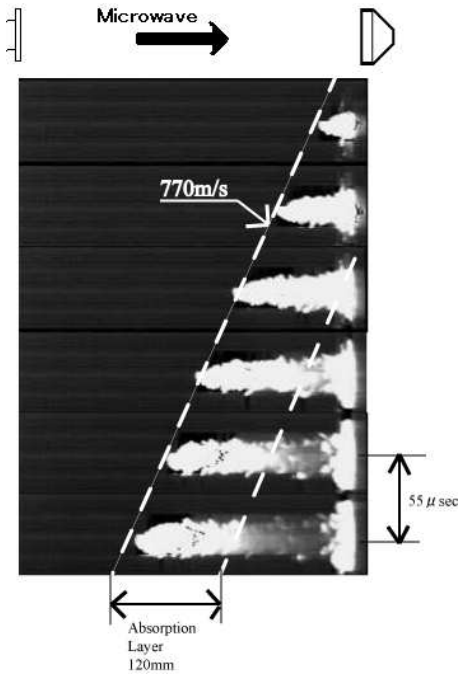

Figure 4.1: Framing photographs of plasma propagation. P=840kW, 110GHz, τ=0.4ms, 18,000FPS

Figure 4.2 shows velocity dependency on microwave power density. The velocity increases with power density.

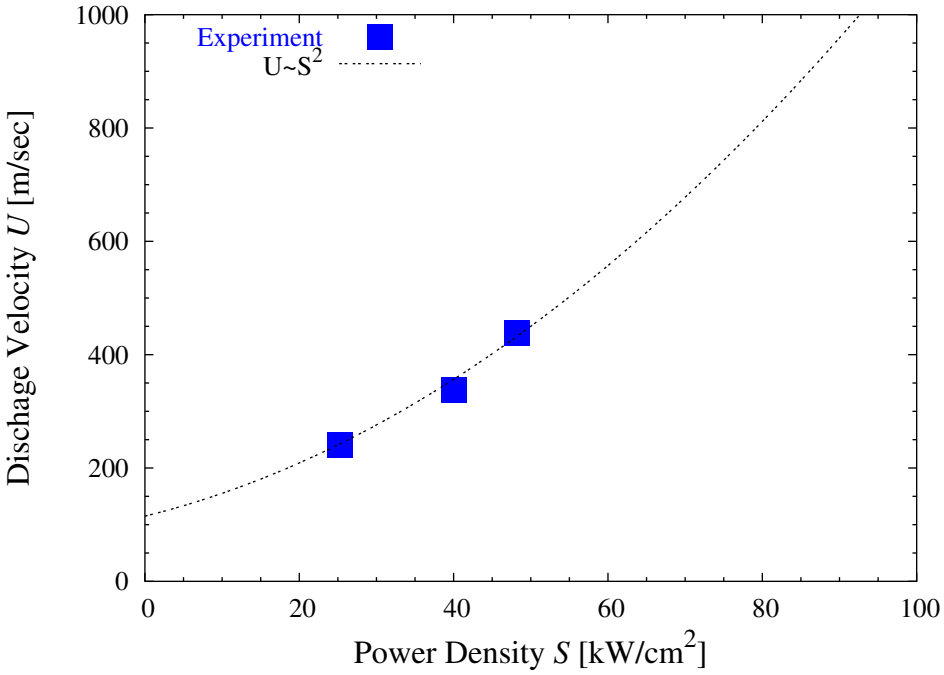

Figure 4.2: Dependence of plasma front velocity U on microwave power flux density S, 170GHz

Measured velocity shows good agreement with theoretical researches in Russia mentioned in section 2.1.

Low ambient pressure experiments

Figure 4.3 shows the dependence of propagation velocity on ambient pressure. As shown in the figure, the propagation velocity increases with decrease in ambient pressure.

Calculation result by the theory at section 2.2 is plotted, on the same figure. It showed a good agreement with measured ones.

4.1.2 Discharge front propagation inside a 2-D parabola reflector

A 2-dimensional parabola reflector was used for visualization of plasma development in the thruster. Figure 4.4 shows pictures of plasma development inside the 2-D reflector. As seen in the figure, plasma propagates in three directions. These propagations can be classified into two groups; a branch on the left hand side and two spokes on the right hand side. The left branch absorbs the microwave beam power directly and glows up to a big branch.

On the other hand, two small spokes absorb the microwave reflected on the parabola reflector. The power density of reflected microwave is very high at the timing of ignition,

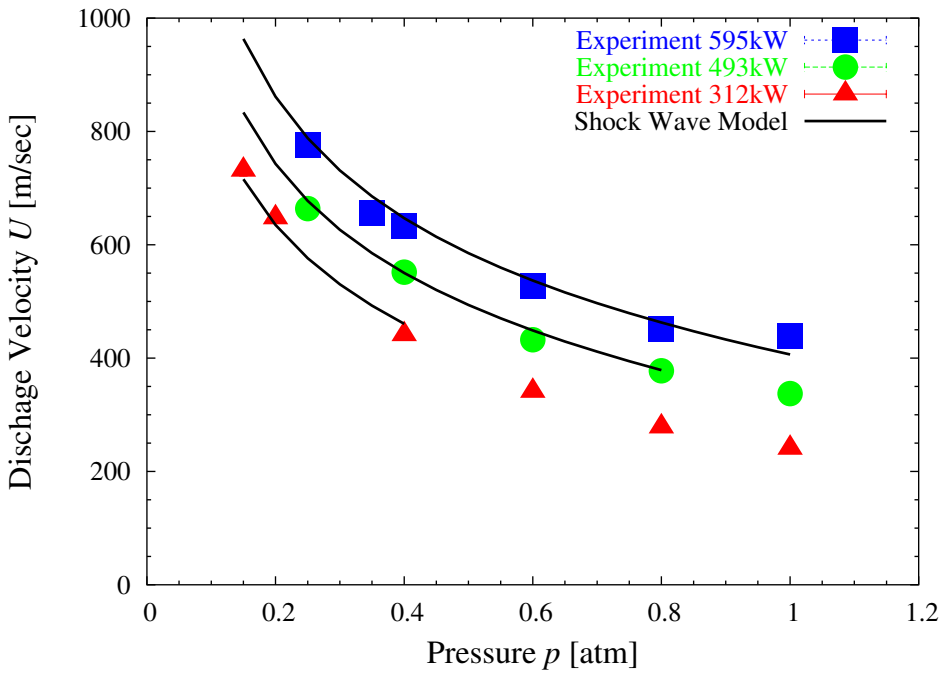

Figure 4.3: Dependence of propagation velocity of plasma front on ambient pressure p_a, 170GHz

though it decreases with time due to the diverging nature of the focused beam and due to the increase in fractional absorption by the left branch plasma as illustrated in Fig.4.5. To say, the spokes are supported by leak power and cannot be a big branch. Consequently, 25μsec after the ignition, the microwave energy would not efficiently used to enhance shock waves directed to the reflector, which will give the main thrust.

4.1.3 Plasma ignition in a parabola reflector

Images of plasma development inside an axsymmetric parabola reflector were taken using a high-speed camera. The parabola's focal length and diameter were 15mm and 90mm, respectively.

Figures 4.6 and 4.7 show the initial discharge stage. The ignition occurred at the focal point of reflector and discharge plasma expands spherically.

4.1.4 Shock wave expansion in a parabola reflector

The propagation velocity of shock waves directed to the reflector was measured. The shock arrival time on the gauges is plotted in 4.8. Deduced average shock-propagation velocity was of the same order of the discharge front propagation speed.(See Figure 4.2) This suggests that there might be some interaction between the shock wave and the discharge front.

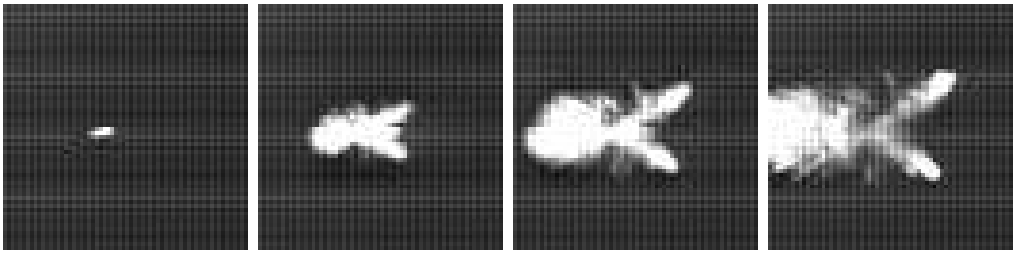

t=0 (μsec) t=25 (μsec) t=50 (μsec) t=75 (μsec)

Figure 4.4: Framing photographs of plasma development in a 2-D reflector. 170GHz, P=1MW, 40,500FPS

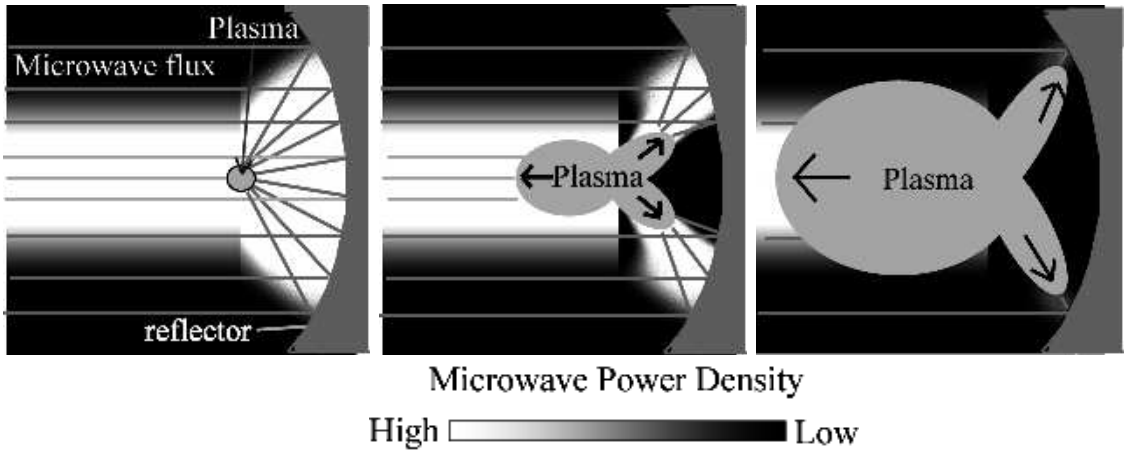

Figure 4.5: Schematic of plasma propagation in a 2-D reflector

The shock propagation velocity varied depending on the distance from the focal point and on the angle from the optical axis. This would be because of the spatial and temporal variation of the microwave power density as illustrated in Fig.4.5.

Figure 4.9 shows the dependence of shock arrival time on microwave pulse duration. Long pulse did not contribute to the enhancement of shock waves at all.

Low ambient pressure experiments

Average velocity of shock wave was also measured in the reduced atmosphere. Figure 4.10 shows average shock velocity, detected with pressure gauge A.(Fig.3.22) It had the same dependence on pressure with plasma propagation velocity.

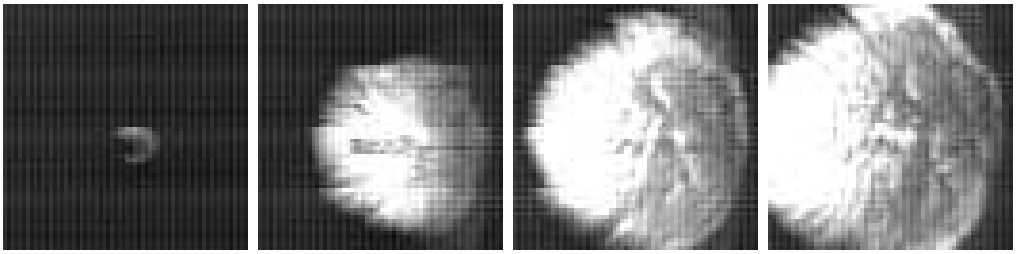

t=0 (μsec) t=25 (μsec) t=50 (μsec) t=75 (μsec)

Figure 4.6: Framing photographs of plasma development in parabolic reflector. 170GHz, P=730kW, 40,500FPS

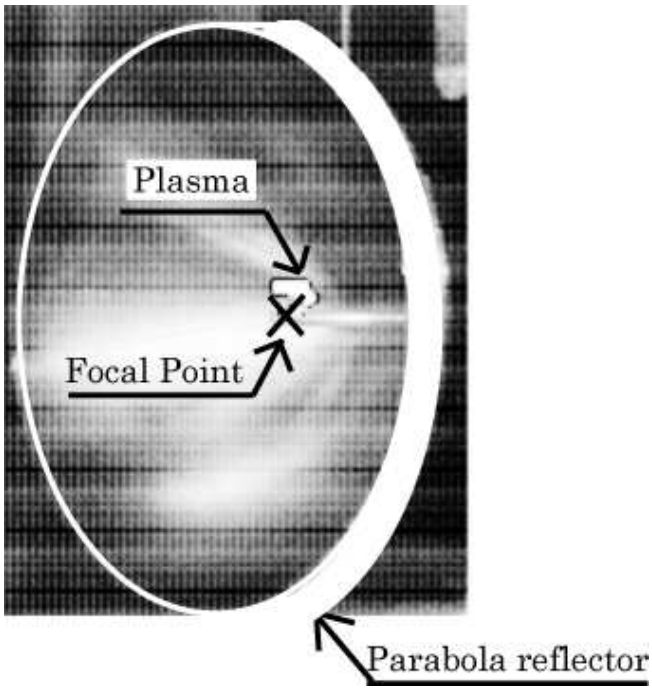

Figure 4.7: Initial plasma development inside a parabola.

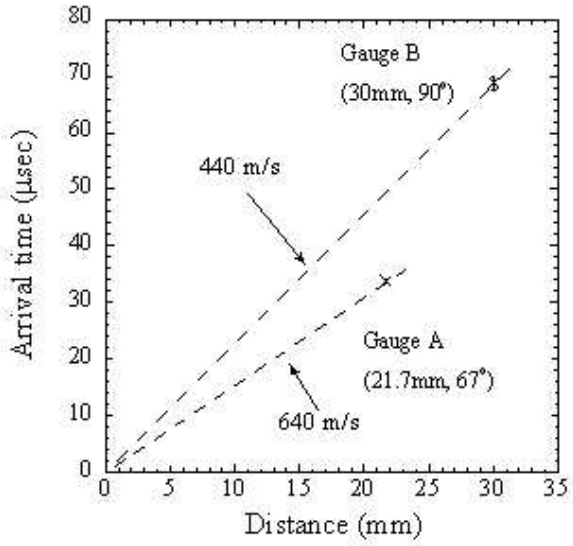

Figure 4.8: Dependence of the shock wave arrival time on distance from focal point. P=930kW, 170GHz

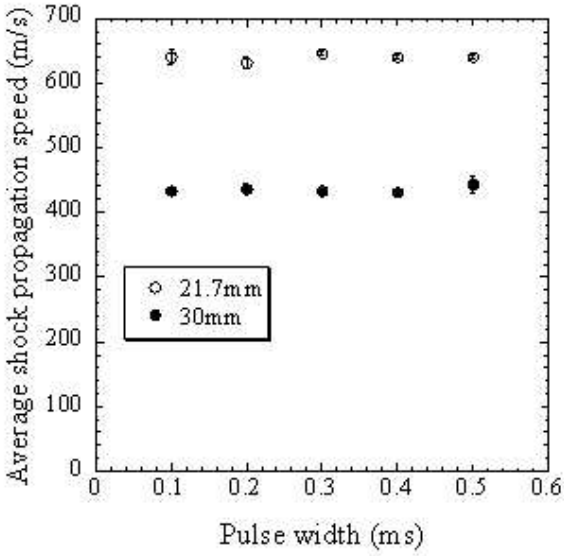

Figure 4.9: Dependence of the shock wave velocity on pulse width. P=930kW, 170GHz

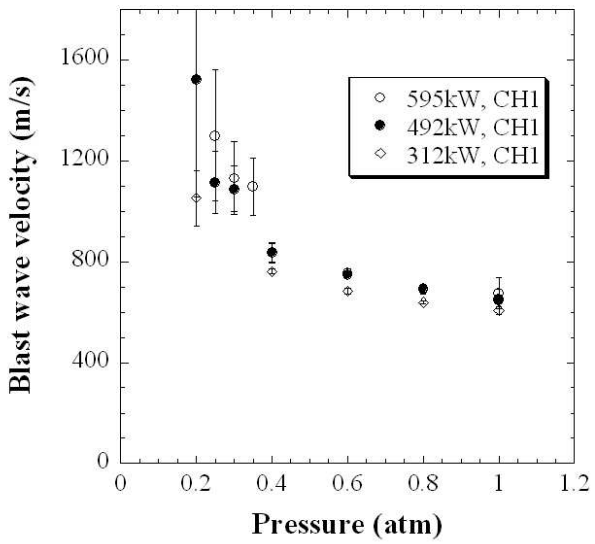

Figure 4.10: Dependence of shock wave velocity on ambient pressure p_{a}.

4.2 Thrust Measurement

4.2.1 Dependence on Power and Pulse Width

Figure 4.11 shows the propulsive impulse obtained with the parabola thruster model. Impulse increased with microwave pulse width τ and power P. However for long τ, increment of impulse becomes small.

Figure 4.12 shows the momentum coupling coefficient C_{m}, defined as,

$$C_{\mathrm{m}} = \frac{I}{P\tau} \tag{4.1}$$

As show, C_{m} decreased with τ. This would be because, in the long pulse case, most of the energy was provided to the plasma developed outside of the parabola and the pressure of the plasma was not converted to the thrust.

On the other hand, C_{m} was found independent on P.

4.2.2 Dependence on Thruster Length

Figure 4.13 shows measured impulse and figure 4.14 shows coupling coefficient for cone-cylinder thruster model at P=635kW. Both graphs contains short pulse(100μsec) result and long pulse (400μsec) result.

C_{m} increased monotonically with length of cylinder L in long pulse condition. However, C_{m} slightly decreased in short pulse condition.

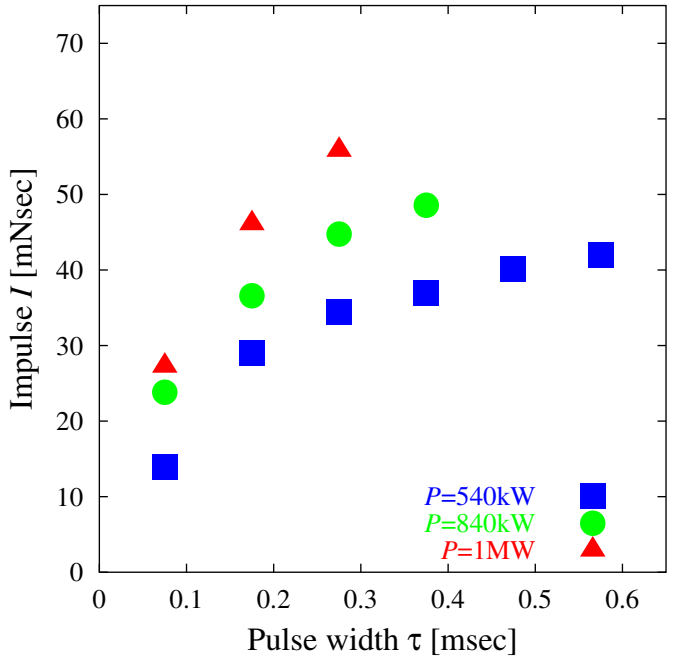

Figure 4.11: Dependence of impulse on pulse width τ. 170GHz, P=540kW-1MW, parabola thruster model

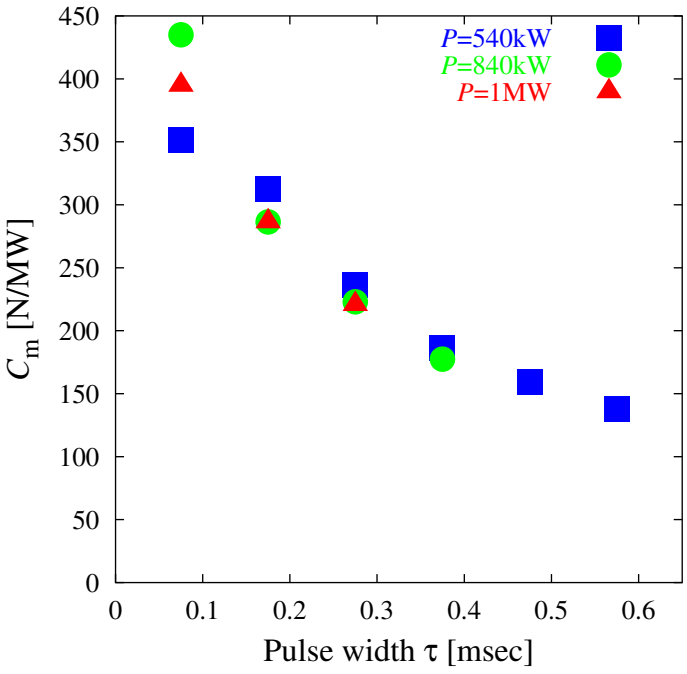

Figure 4.12: Dependence of C_m on pulse width τ. 170GHz, P=540kW-1MW, parabola thruster model

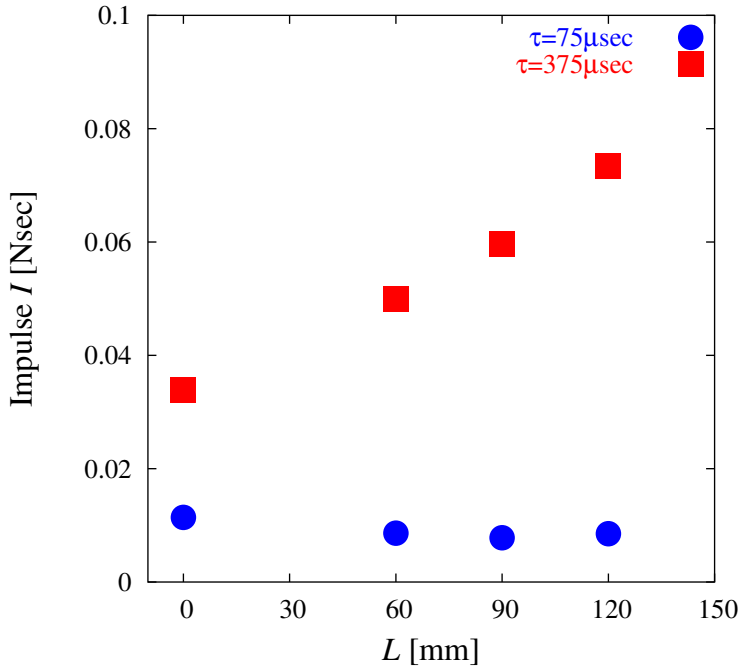

Figure 4.13: Dependence of impulse on thruster length L. 170GHz, P=657kW, Cone-cylinder thruster models

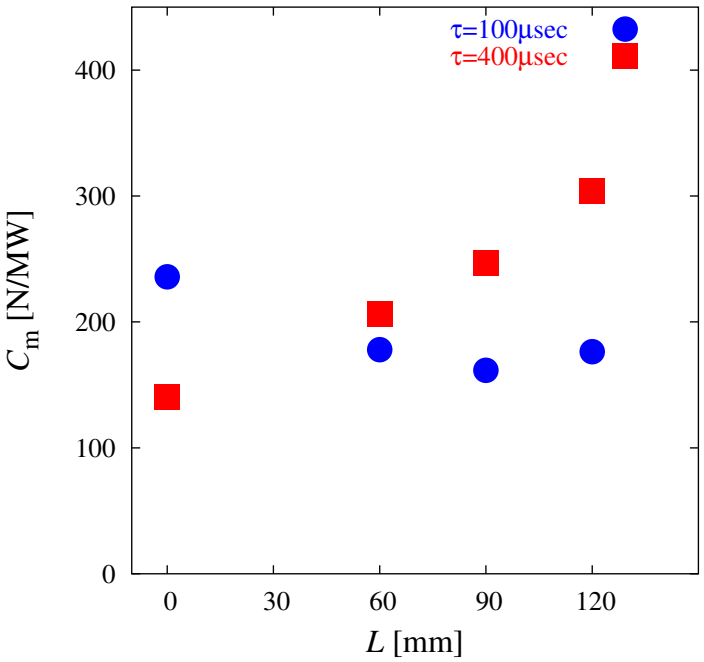

Figure 4.14: Dependency of C_m on Thruster Length L. 170GHz, P=657kW, Cone-cylinder thruster models

4.2.3 Dependence on Ambient Pressure

The dependence of thrust on ambient pressure was examined, using a reduced pressure chamber. The parabolic thruster model was used. The ambient pressure was reduced from 1atm (atmospheric pressure) to 0.1atm.

Figure 4.15 and 4.16 shows the measured impulsive thrust under varied ambient pressure and pulse width at P=595kW and P=312kW. The measured impulse had a peak and the optimum pressure was increased with pulse duration.

At P=595kW, anomalous discharge was observed outside of the thruster and thrust was not detected at the pressure below 0.3atm. At P=312kW, thrust was not detected at the pressure below 0.1atm.

Figure 4.17 and 4.18 shows the momentum coupling coefficient C_{m}. As same as impulse, C_{m} had a peak for pressure. The optimum pressure was increased with pulse duration and power.

However, dependence of thrust performance on ambient pressure is found weaker than that on the pulse duration.

4.3 Effect of thruster scale

When the microwave pulse width is long, plasma generated in the thruster model protrudes from the nozzle and its front propagates towards the beam source through microwave channel.

Figure 4.19 shows a typical photograph of large developed plasma. As shown in Fig.4.19, typically plasma develops into a long cylindrical shape and its axial length varied with pulse condition and ambient pressure.

On the other hand, C_{m} has also dependence on these conditions. Thrust performance is considered to depend on the relative size of plasma and thruster. As optimum thruster size is decided by scaling rule, scaling parameter plays important role in thruster design work.

Then, scaling parameters Λ is defined as ratio of the thruster size and plasma.

$$\Lambda = \frac{L_{\mathrm{thruster}}}{L_{\mathrm{plasma}}} \tag{4.2}$$

$$L_{\mathrm{plasma}} = U(S)\tau \tag{4.3}$$

Here, L_{thruster} and L_{plasma} are defined as axial length of the thruster and plasma, respectively. L_{plasma} is calculated from velocity of plasma propagation $U(S)$ and pulse duration τ.Their configurations are shown in Fig.4.20. In Fig.4.20, D_{thruster} and d_{plasma} are defined as diameter of the thruster and plasma, respectively.

4.3.1 Dependence on scale parameter

Figure 4.21 shows dependence of C_{m} of cone-cylinder type thruster on the scale parameter.

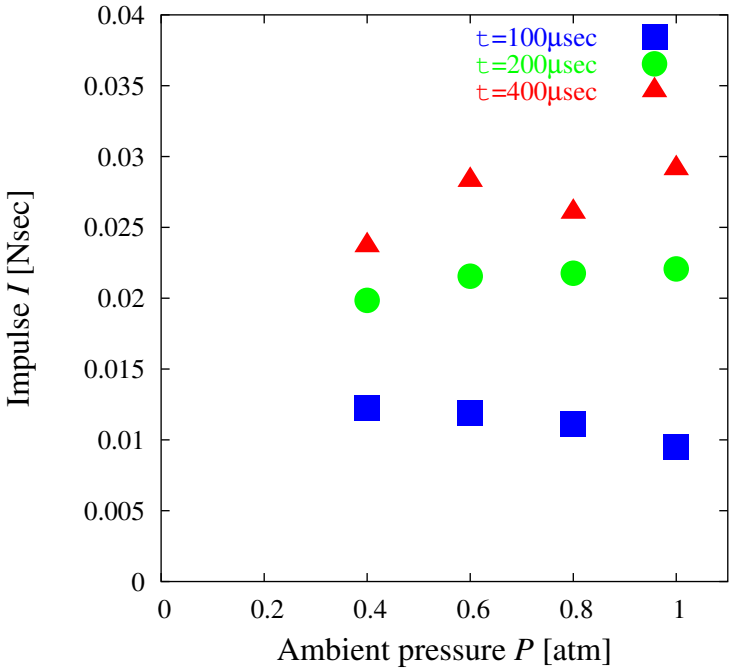

Figure 4.15: Dependence of impulse on pressure p_a. 170GHz, P=595kW, parabola type

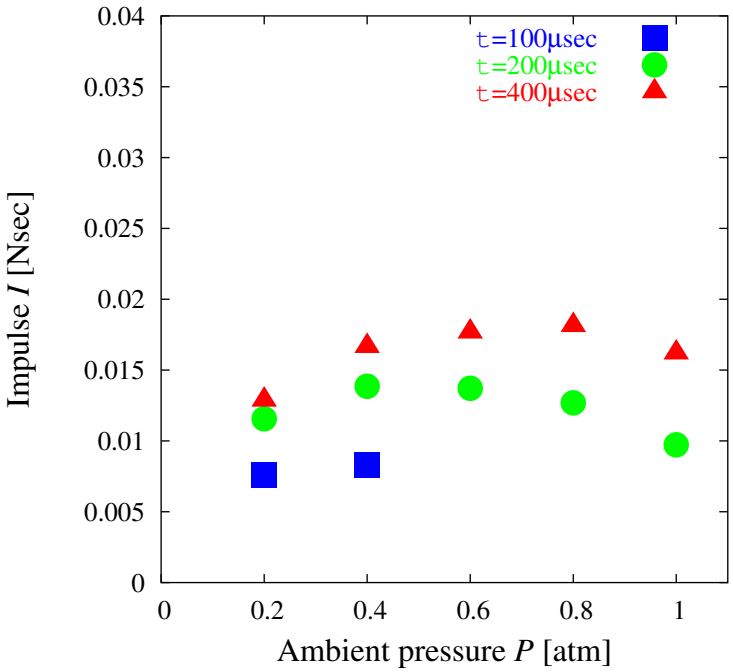

Figure 4.16: Dependence of impulse on p_a. 170GHz, P=312kW, parabola thruster model

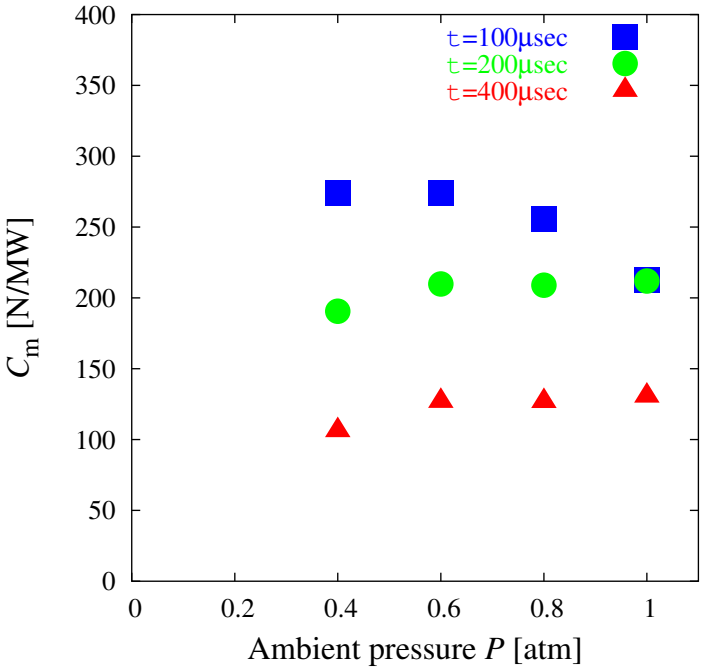

Figure 4.17: Dependence of C_m on pressure p_a. 170GHz, P=595kW, parabola thruster model

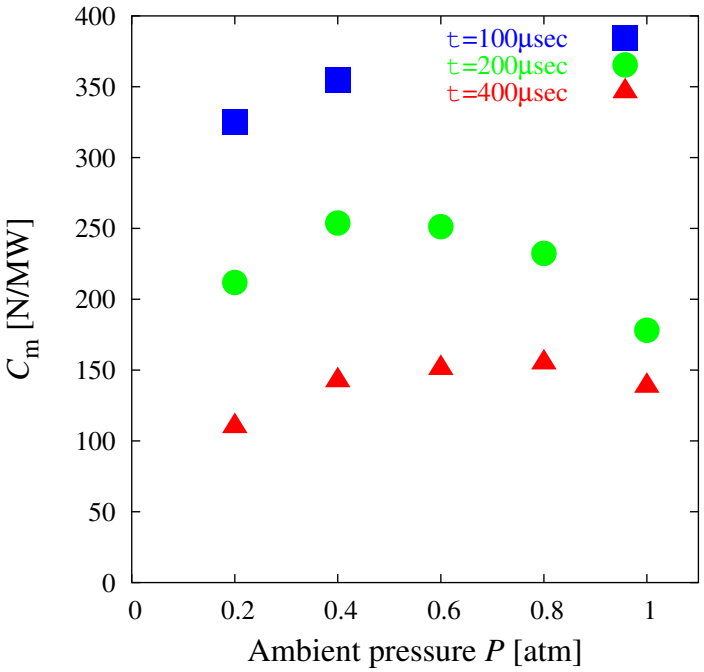

Figure 4.18: Dependence of C_m on pressure p_a. 170GHz, P=312kW, parabola thruster model

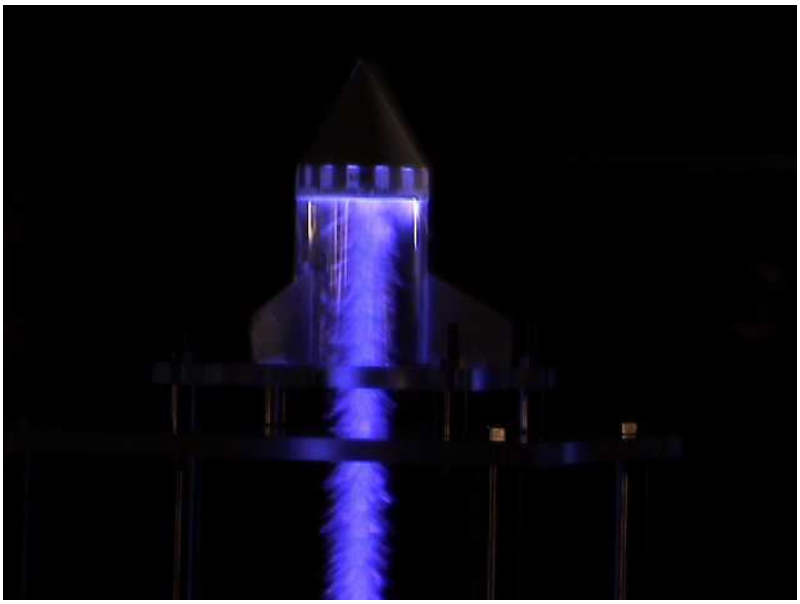

Figure 4.19: Photograph of plasma and cone-cylinder thruster model.

As shown in Fig.4.21, C_{m} has a peak for Λ. For cone-cylinder models, maximum C_{m} is gained at $\Lambda \sim 1$.

In the region $\Lambda \leq 1$, the late part of the microwave pulse power is absorbed at outside of the thruster. Then the plasma expands far from the nozzle surface. Only limited microwave power is converted to thrust and C_{m} decreases. Effective microwave power is limited to absorbed ones inside the thruster.

In the region $\Lambda \geq 1$, whole microwave power is absorbed in the thruster. However, C_{m} also decreases.

Experimental and computational research on RP laser propulsion reveals the process of thrust decline in long nozzle thruster. Absorbed energy by plasma drives a blast wave and the blast wave expands along the nozzle wall. Through the expansion and exhaust process, pressure in the nozzle declines lower than atmospheric pressure. Pressure inversion between the inside and the outside of the nozzle induces air-refill process and produces negative thrust. The pressure recovers through the air-refill process. The large thrusters take long time in refill process and total thrust performance declines. [21]

Figure 4.22 shows C_{m} dependency on Λ in the case of parabolic thruster. As parabolic thruster is shorter than cone-cylinder type, the graph shows only region of $\Lambda \leq 1$. In parabolic thruster, peak of C_{m} appears at $\Lambda \sim 0.5$.

Figure 4.22 shows C_{m} dependence on Λ in the case of parabolic thruster. As parabolic thruster is shorter than cone-cylinder type, the graph shows only region of $\Lambda \leq 1$. In parabolic thruster, peak of C_{m} appears at $\Lambda \sim 0.5$.

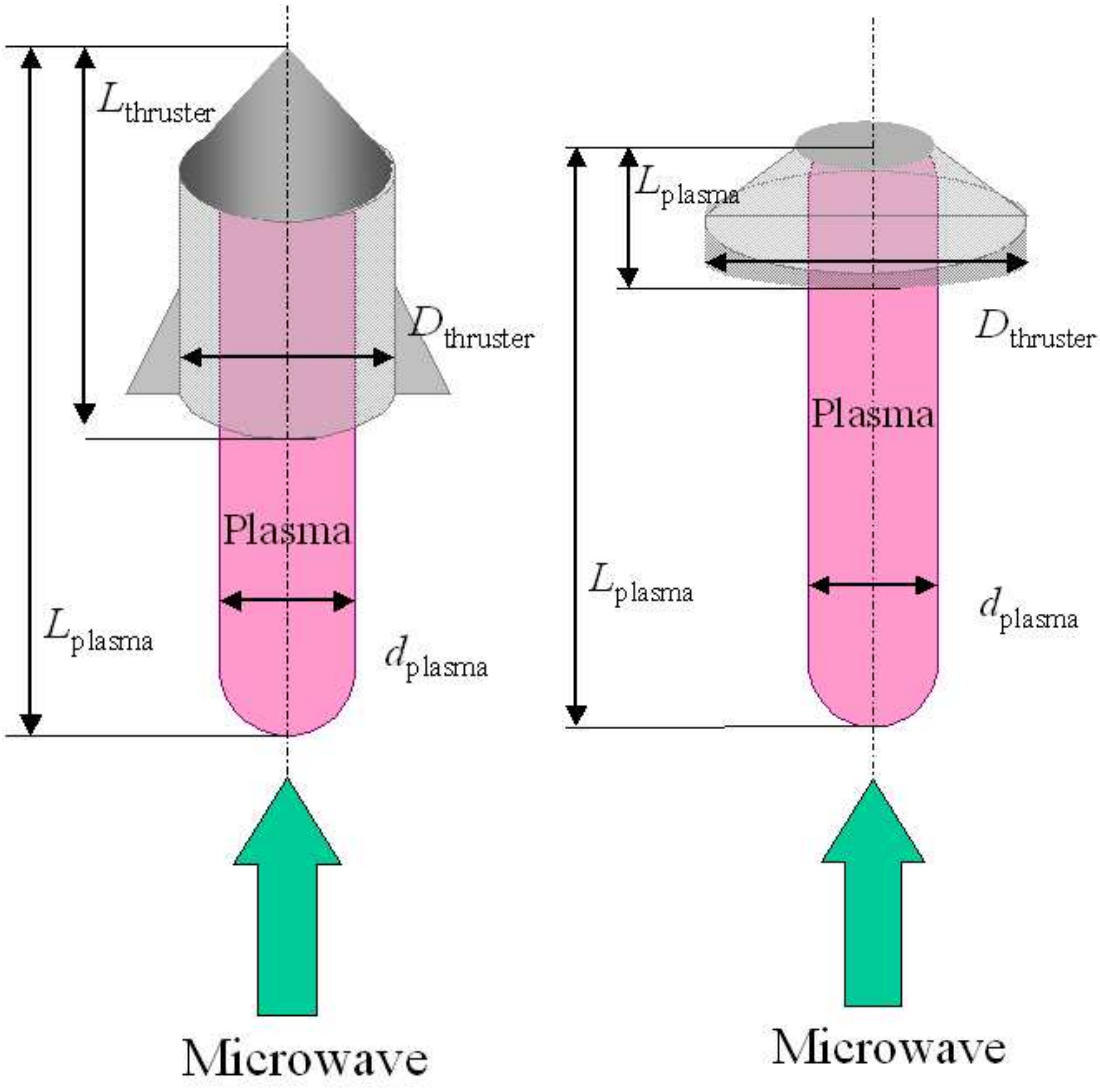

Figure 4.20: Configuration of relative scale of plasma and thruster model

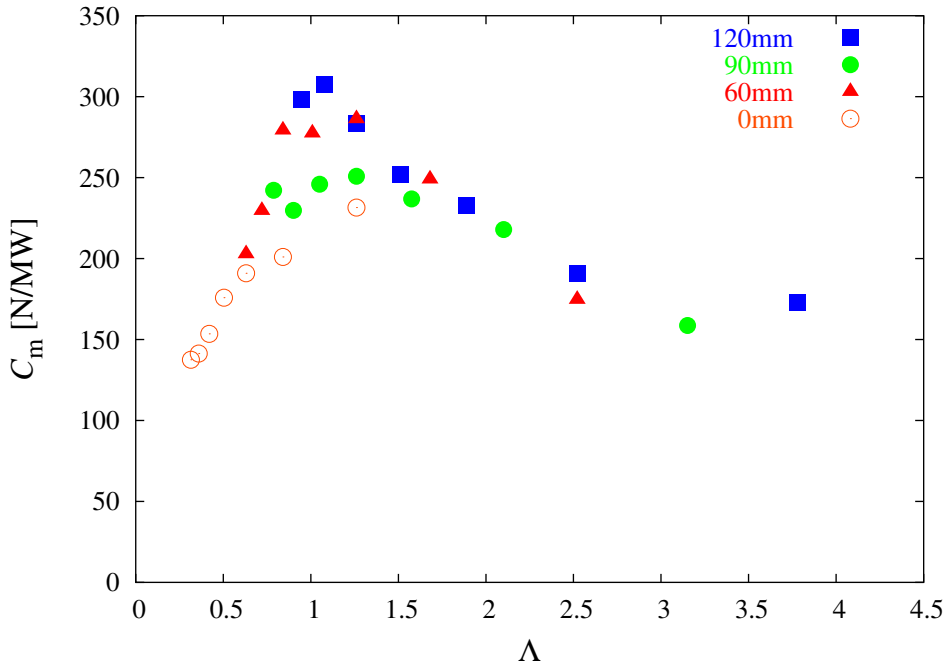

Figure 4.21: Dependence of C_m on Λ cone-cylinder thruster models. P=673kW

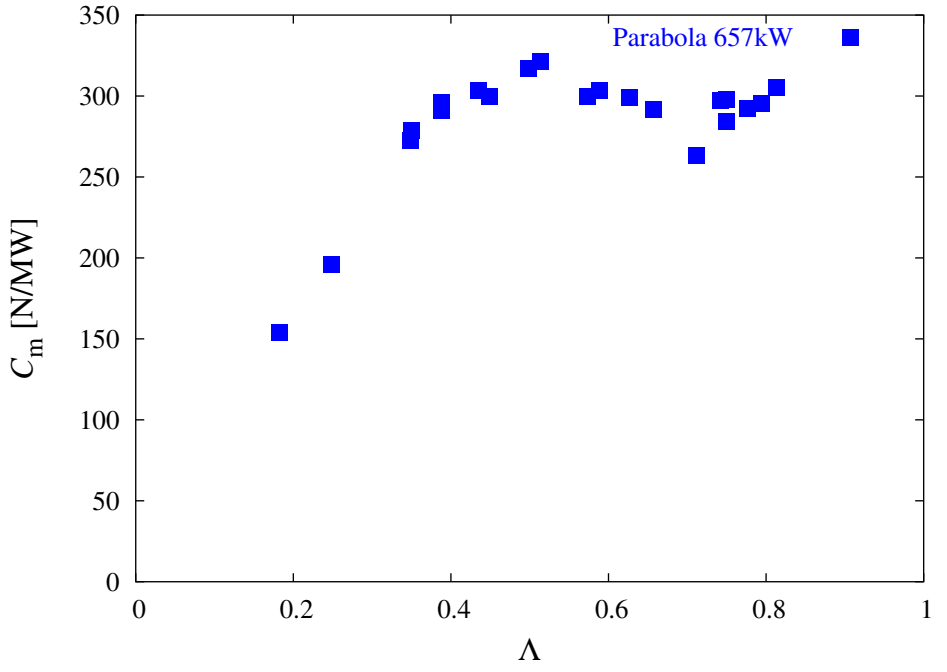

Figure 4.22: Dependence of C_m on Λ parabola thruster model. P=673kW

4.3.2 Thruster shape

The maximum C_{m} was gained at different Λ_{peak} between cone-cylinder thruster models and parabola thruster model. The exit diameter of a parabola thruster model is larger than that of cone-cylinder thruster models. Indeed, the diameter of plasma d_{plasma} is same in both thrusters. Table 4.1 lists the comparison of Λ_{peak} for parabola thruster model and cone-cylinder thruster models.

Thruster type	d_{plasma} (mm)	D_{thruster} (mm)	Λ_{peak}
Parabola	46	90	0.5
Cone-Cylinder	46	60	1.0

Table 4.1: Comparison of Λ_{peak} of parabola thruster and cone-cylinder thruster

Λ_{peak} increases with D_{thruster} decrease. Λ_{peak} dependence on exit diameter is explained as the following. When radial scale is large enough, the blast wave driven by plasma also expands to radial direction. Thus, more energy of the blast wave is converted to thrust than small thruster. To say, large radial scale thrusters gain the marginal expansion of a blast wave.

However, it is difficult to describe the behavior of the blast wave caused by axially long cylinder shaped plasma. To deal exactly, it is necessary to carry out the computational examination.

4.3.3 Ambient pressure effect

Figures 4.23 and 4.24 show C_m dependency on Λ in the case of reduced ambient pressure with parabolic thruster.

As ambient pressure decrease, Λ_{peak} slightly increase and maximum C_{m} increase.

When ambient pressure becomes low, expanded air volume becomes large. Then, fractional scale of the nozzle to plasma becomes small.

4.4 Multipulse Operation

Microwave pulses were injected in the 60 or 100Hz repetition rate. Plasma was ignited succusessfully for each pulse. Figure 4.25 shows repetition of plasma ignition. The velocity of plasma propagation was measured using a high-framing speed camera. Coupling coefficient at each pulse was also measured using conical thruster models.

4.4.1 Plasma Propagation

The propagation velocity of plasma under multi pulse operation was plotted in Fig. 4.26.

As seen in Fig.4.26, the propagation velocity at latter pulse shot was faster than that of first pulse shot. In the case of third pulse in 100Hz repetition rate, the measured velocity

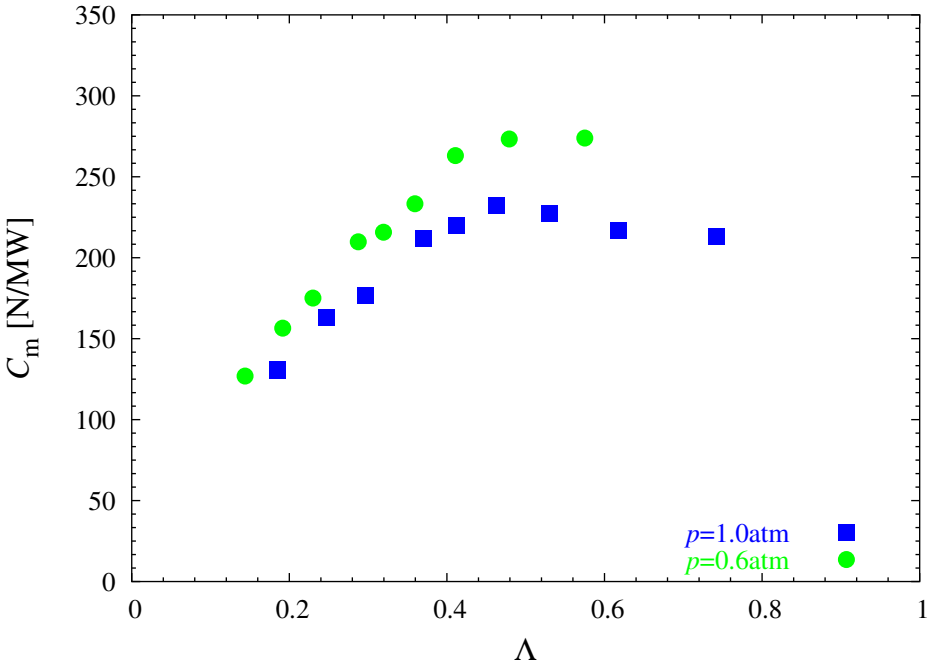

Figure 4.23: Dependence of C_m on Λ parabola thruster model. P=593kW

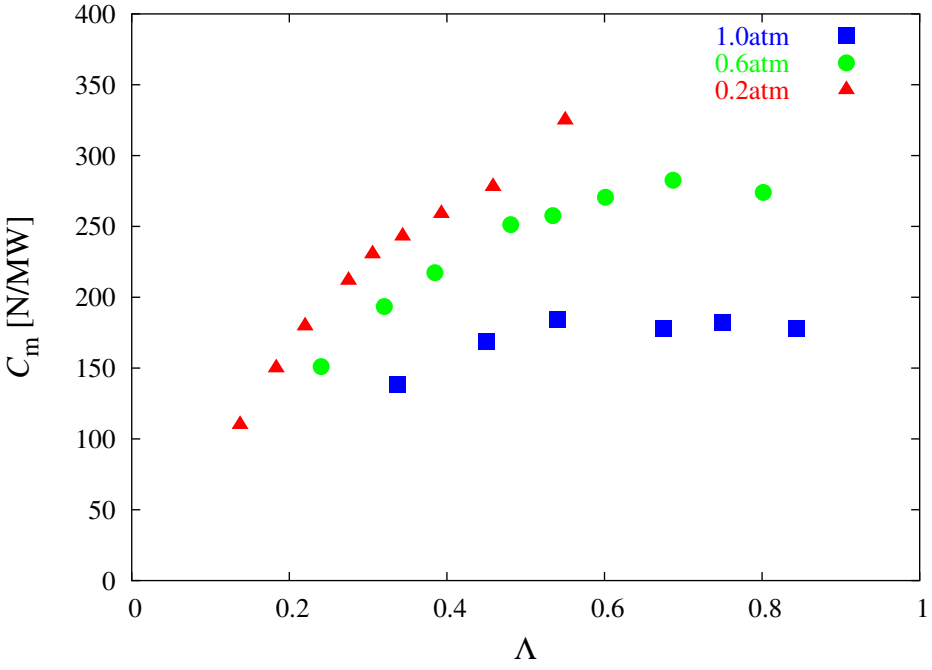

Figure 4.24: Dependence of C_m on Λ parabola thruster model. P=312kW

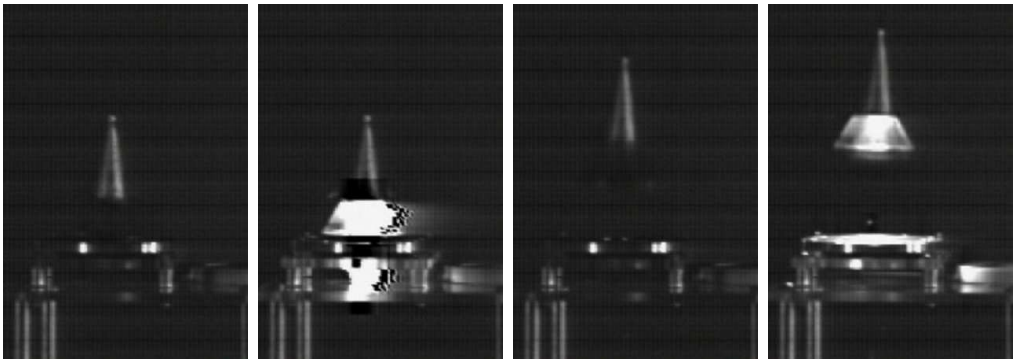

t=0 (msec) t=1 (msec) t=10 (msec) t=21 (msec)

Figure 4.25: Framing photographs of repetitive plasma ignition. 170GHz, 60Hz repetition

was nearly double of that at single pulse condition. This would be because, in the latter shot, the air in the microwave channel remains hot and its density is lowered.

4.4.2 Thrust Measurement

Thurst measurement under multipulse operation was conducted, using cone thruster model.

A non-dimensional scaling parameter r was used.

$$r = \frac{R_n}{R^*} \tag{4.4}$$

Here, R^* expresses the strength of an explosive source as

$$R^* = \left(\frac{E_1}{p_a \sin^2(\alpha/2)} \right)^{1/3} \tag{4.5}$$

where E_1 is defines as input energy and p_a expresses atmospheric pressure. R^* is the radius of a shock front when the post-shock pressure decays to the level of atmospheric pressure.[22]

Measured C_m is plotted in Fig.4.27 and 4.28 for various α and r. As shown in figures, C_m increases with r. This indicates that the optimum nozzle length r_opt is larger than 0.6 for τ=1msec condition. In addition, C_m is decreased with α. This is because the pressure recovery in the air-refresh process becomes slow and inefficient with an increase in α.

The coupling coefficient at the second pulse $C_{\mathrm{m}2}$ is lower than that at first pulse $C_{\mathrm{m}1}$ for all the thruster configurations.

A ratio of coupling coefficients $C_{\mathrm{m}2}/C_{\mathrm{m}1}$ was plotted in Fig. 4.29.

As shown in the Fig.4.29, $C_{\mathrm{m}2}/C_{\mathrm{m}1}$ kept low at 100Hz repetition. This indicates that 100Hz repetition rate is too high to completely scavenge the air inside the nozzle. If the scavenging takes longer time than the pulse interval, following pulse is shoot into the hot air remained inside of the nozzle. Through the computational research on pulsed laser

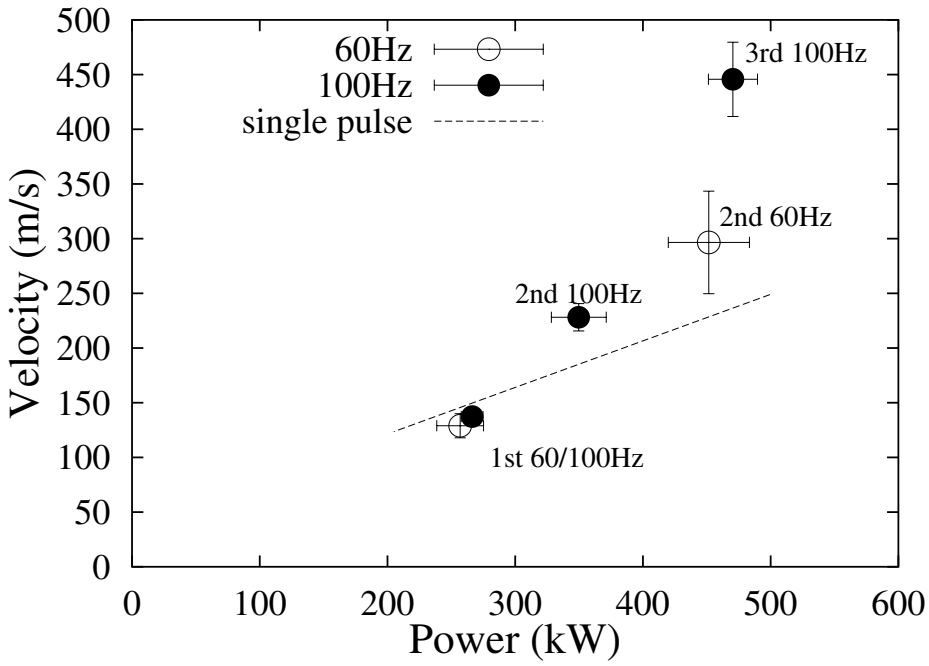

Figure 4.26: Dependence of plasma propagation velocity on power and repetition rate.

propulsion, after the exhaust process, mass of air inside of the nozzle reduces and it takes long time for recovery.

However, to the dependence of C_{m1} on r was dominant over the dependence of $C_{\mathrm{m2}}/C_{\mathrm{m1}}$ and higher C_{m2} was achieved at larger r. This indicates that thruster design guideline acquired through the single-pulse experiments is still helpful for pulse repetitive operation.

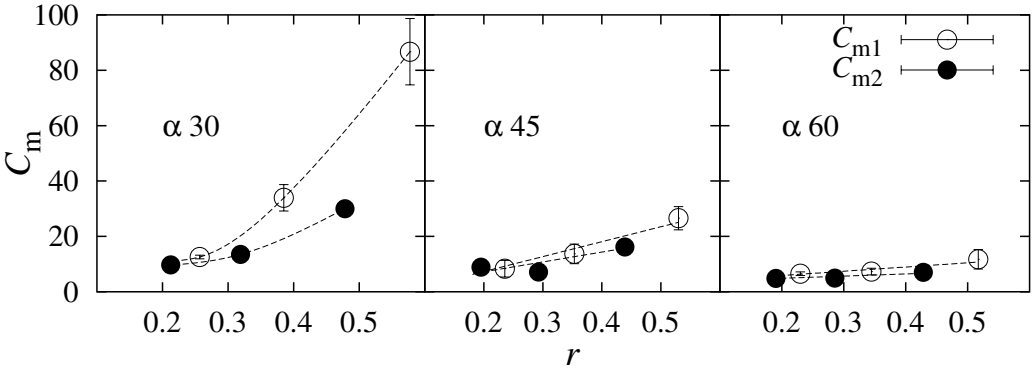

Figure 4.27: Dependence of C_{m} on α and r at 60Hz repetition.

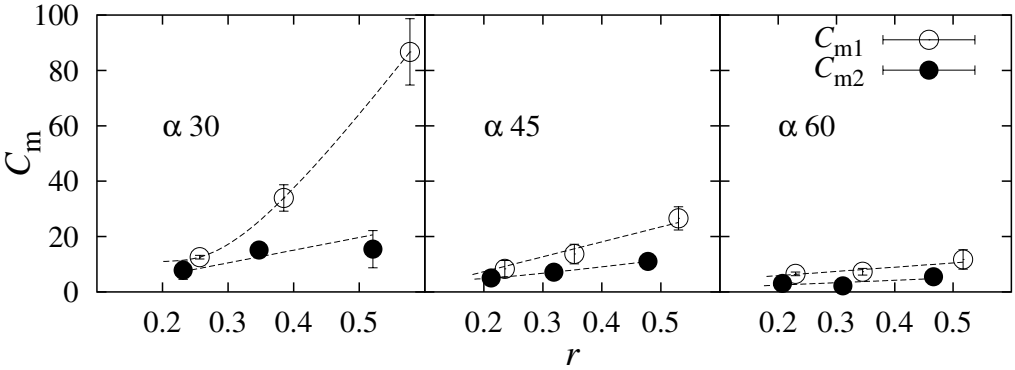

Figure 4.28: Dependence of C_{m} on *alpha* and r at 100Hz repetition.

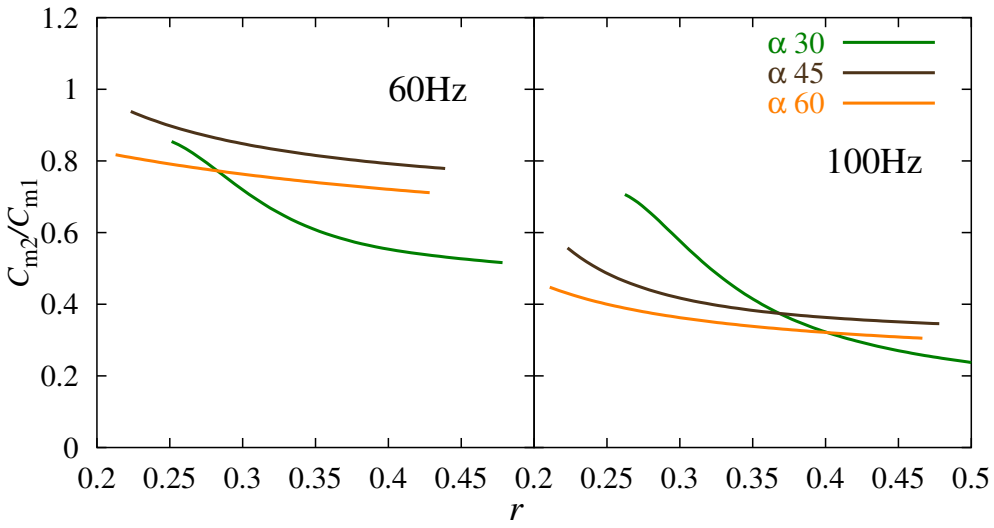

Figure 4.29: Dependence of C_{m2}/C_{m1} on α and r.

Chapter 5

Conclusion

An experimental study of microwave beaming propulsion was conducted using a high power gyrotron. The observation of plasma development and shock wave propagation in the thruster and thrust measurement using three types of thruster models were conducted.

Plasma and shock wave observation

Plasma propagates towards radiation source of microwave with constant velocity. Its velocity depends on power and ambient pressure. Experimental results were well agreed with theoretical prediction.

In the 2-D parabola reflector, plasma was found to develop in three directions during the initial plasma development stage. In the later stage, only the plasma leaving from the reflector was developed while the plasma expanding toward the reflector was not enhanced.

Shock propagation speed measurement in the axsymmetric parabola reflector suggested that there might be some supersonic interaction between the shock and discharge front.

Thrust measurement

Thrust measurement was conducted using a parabola thruster model and cone-cylinder thruster model. The dependence of momentum coupling coefficient C_{m}, a ratio of thrust and input power, on pulse width, power, length of thruster nozzle, and ambient pressure was deduced.

For the aspect of general dependence of C_{m} on the thruster shape, the scaling parameter Λ, the fractional ratio of thruster length and plasma length, was applied. C_{m} had a peak for axial ratio Λ. Λ_{opt} was varied with radial ratio and ambient pressure.

Multi pulse operation

For examination of pulse repetition, microwave pulses were injected repetitively. The observation of plasma development and thrust measurement were carried out.

The measured velocity of plasma propagation in the multi pulse condition became faster than that in the single pulse condition, and higher velocity was obtained at higher repetition rate due to the hot air remaining on the way of microwave channel.

Thrust measurement was conducted using a thruster models with conical nozzle. Thurst was calculated using a record of flight trajectory, pulse by pulse.

Coupling coefficient at latter pulse shot was lower than at single pulse. Dependence of $C_{\mathrm{m2}}/C_{\mathrm{m1}}$ on a scale parameter r, ratio of nozzle length and expanded radius of plasma, was contrary to the dependence of C_{m1} on r. However, to the dependence of C_{m1} on r was dominant over the dependence of $C_{\mathrm{m2}}/C_{\mathrm{m1}}$ and higher C_{m2} was achieved at larger r. This indicates that thruster design guideline acquired through the single-pulse experiments is still helpful for pulse repetitive operation.

Bibliography

[1] Kantrowitz. Propulsion to orbit by ground-based lasers. *Astronautics and Aeronautics*, 10(5):74–76, May 1972.

[2] L.N. Myrabo, D.G. Messitt, and F.B. Mead Jr. Ground and flight tests of a laser propelled vehicle. AIAA Paper No. 98-1001, American Institute of Aeronautics and Astronautics, 1998.

[3] L.N. Myrabo. World record flights of beamed-riding rocket lightcraft: Demonstration of disruptive propulsion technology. AIAA Paper No. 2001-3798, American Institute of Aeronautics and Astronautics, 2001.

[4] J.L. Schad and J.J. Moriarty. Microwave rocket concept. In *XVI International Astronaut Congress*, pages 175–199. Athens, 1965.

[5] J.P. Knecht and M.M. Micci. Analysis of a microwave-heated planar propagationg hydrogen plasma. *AIAA JOURNAL*, 26(2):188–194, 1988.

[6] T. Nakagawa, Y. Mihara, K. Komurasaki, K. Takahashi, K. Sakamoto, and T. Imai. Propulsive impulse measurement of a microwave-boosted vehicle in the atmosphere. *Journal of Spacecraft and Rockets*, 41(1):151–153, 2003.

[7] K.L.G. Parkin and F.E.C. Culick. Feasibility and performance of the microwave thermal rocket launcher. In Kimiya Komurasaki, editor, *Beamed Energy Propulsion: Second International Symposium on Beamed Energy Propulsion*, pages 407–417. American Institute of Physics, 2003.

[8] H. Katsurayama, M. Ushio, K. Komurasaki, and Y. Arakawa. Analytical study on flight performance of an air-breathing RP laser launcher. AIAA Paper No. 2004-3585, 40th AIAA/ASME/SAE/ASEE Joint Propulsion Conference and Exhibit, 2004.

[9] H. Katsurayama, K. Komurasaki, A. Momozawa, and Y. Arakawa. Numerical and engine cycle analyses of a pulse laser ramjet vehicle. *Transactions of the Japan Society for Aeronautical and Space Sciences, Space Technology Japan*, 1:9–16, 2003.

[10] A.V. Gaponov-Grekhov and V.L. Granatstein, editors. *Applications of High-Power Microwaves*, pages 1–24. Artech House, INC, 1994.

[11] M. Thumm. Progress in gyrotron development. *Fusion Engineering and Design*, 66:69–90, 2003.

[12] K. Sakamoto. Application of plasma heating technology for fronteir science. In *Proceedings of Plasma Science Symposium 2005 and The 22nd Symposium on Plasma Processing*, 2005.

[13] A.V. Gaponov-Grekhov and V.L. Granatstein, editors. *Applications of High-Power Microwaves*, pages 147–156. Artech House, INC, 1994.

[14] Yu. P. Raizer. Propagation of high-pressure microwave discharege. *Soviet Physics JETP*, 34(1):114–120, January 1972.

[15] Yu.Ya. Brodskii, S.V. Golubev, V.G. Zorin, A.G. Luchinin, and V.E. Semenov. New mechanism of gasdynamic propagation of a discharge. *Soviet Physics JETP*, 57(5):989–993, May 1983.

[16] A.L. Vikharev, A.M. Gorbachev, O.A. Ivanov, and A.L. Kolysko. Plasma parameters and stimulated uv emission of filamentary structures in a high-pressure microwave discharge. *JETP*, 79(1):94–101, July 1994.

[17] V.M. Batenin, I.I. Klimovskii, G.V. Lysov, and V.N. Troitskii, editors. *Superhigh Frequency Generators of Plasma*, pages 97–109. CRC Press, Inc, 1994.

[18] L.D. Landau and E.M. Lifshitz. *Fluid Mechanics*, volume 6 of *Landau and Lifshitz:Course of Theoretical Physics*, pages 489–494. Butterworth-Heinemann, 2nd english edition, 1984.

[19] K. Sakamoto, A. Kasugai, M. Tsuneoka, K. Takahashi, and T. Imai. High power 170GHz gyrotron with synthetic diamond window. *Review of scientific instruments*, 70(1):208–212, 1999.

[20] A. Kasugai, K. Sakamoto, R. Minami, K. Takahashi, and T. Imai. Study of millimeter wave high-power gyrotron for long pulse operation. *Nuclear Instrument and Method in Physics Research A*, 528:110–114, 2004.

[21] Y. Hirooka, H. Katsurayama, K. Komurasaki, and Y. Arakawa. Nozzle performance of a RP laser thruster. AIAA Paper No. 2003-4429, 39th AIAA/ASME/SAE/ASEE Joint Propulsion Conference and Exhibit, 2003.

[22] K. Mori, H. Katsurayama, Y. Hirooka, K. Komurasaki, and Y. Arakawa. An experimental study on the energy balance in the repetitively pulsed laser propulsion. AIAA Paper No. 2003-0496, 41st Aerospace Science Meeting and Exhibit, 2003.

修士論文に関する発表一覧

[1] 小田 靖久, 中川 樹生, 小紫 公也, 高橋 幸司, 春日井 敦, 坂本 慶司, 今井 剛: “マイクロ波ロケット内部のプラズマ挙動”, プラズマ応用科学 Applied Plasma Science Vol.11 Dec.2003 pp47-52

[2] Yasuhisa Oda, Tatsuo Nakagawa, Kimiya Komurasaki, Koji Takahashi, Atsushi Kasugai, Keishi Sakamoto, and Tsuyoshi Imai: “An observation of plasma inside of microwave boosted thruster”, *Beamed Energy Propulsion: Proceedings of Second International Symposium of Beaming Energy and Propulsion*, Kimiya Komurasaki ed., pp399-406, 2003 Oct., Sendai, Japan

[3] Yasuhisa Oda, Tatsuo Nakagawa, Kimiya Komurasaki, Koji Takahashi, Atsushi Kasugai, Keishi Sakamoto, and Tsuyoshi Imai: “Plasma expansion and shock wave propagation in a microwave-beaming thruster”, *Proceedings of 24th International Symposium on Space Technology and Science*, pp228-233, 2004 Jun., Miyazaki, Japan

[4] Yasuhisa Oda, Masato Ushio, Kimiya Komurasaki, Koji Takahashi, Atsushi Kasugai, and Keishi Sakamoto: “A Multi Pulse Flight Experiment of a Microwave Beaming Thruster”, *Third International Symposium of Beaming Energy and Propulsion*, 2004 Oct., Troy, NY, USA

[5] 小田靖久, 中川樹生, 松井信, 小紫公也, 高橋幸司, 春日井敦, 坂本慶司, 今井剛: “1MW 級ジャイロトロンを用いたマイクロ波推進の飛行実験”,第 47 回宇宙科学技術連合講演会, 2003 Nov., 新潟

[6] 小田靖久, 牛尾正人, 小紫公也, 高橋幸司, 春日井敦, 坂本慶司: “高出力マイクロ波を用いたプラズマ生成と宇宙推進への応用”,電気学会原子力研究会「核融合プラズマを知る操る技術について　技術の広がりと応用」, 2004 Sep., 東京

[7] 小田靖久, 牛尾正人, 小紫公也, 高橋幸司, 春日井敦, 坂本慶司: “マイクロ波ビーミング推進器のマルチパルス化実験”,第 48 回宇宙科学技術連合講演会, 2004 Nov., 福井

[8] 小田靖久, 小紫公也, 高橋幸司, 春日井敦, 坂本慶司: “１MW 級ジャイロトロンを用いたプラズマ生成とマイクロ波ビーミング推進への応用”,プラズマ科学シンポジウム 2005／第 22 回プラズマプロセッシング研究会, pp299-300, 2005 Jan., 名古屋